Title
Fluid Flow Patterns Around a Well or an Underground Drift with Comple x Skin Effects

Journal
Water Resources Research, 27(11)

Authors
Bidaux, P.
Tsang, Chin-Fu

Publication Date
1989-11-01

LBL-28072
Preprint

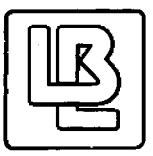

Lawrence Berkeley Laboratory
UNIVERSITY OF CALIFORNIA

EARTH SCIENCES DIVISION

Submitted to Water Resources Research

A Semi-Analytic Study of the Regional Flow Patterns around a Well or an Underground Drift with Complex Skin Effects

P. Bidaux and C.-F. Tsang

November 1989

Prepared for the U.S. Department of Energy under Contract Number DE-AC03-76SF00098.

DISCLAIMER

LBL-28072

A Semi-Analytic Study of the Regional Flow Patterns around a Well or an Underground Drift with Complex Skin Effects

Pascal Bidaux and Chin-Fu Tsang*

Earth Sciences Division
Lawrence Berkeley Laboratory
University of California
Berkeley, California 94720

*Permanent address:
CNRS-URA 1359, Laboratoire d'Hydrogéologie
Université des Sciences et Techniques
Pl. E. Bataillon, 34060 Montpellier Cedex, France

November 1989

This work was supported by the Director, Office of Energy Research, Office of Basic Energy Sciences, Engineering and Geosciences Division, of the U.S. Department of Energy under Contract DE-AC03-76SF00098 and by the Office of Drinking Water, U.S. Environmental Protection Agency, under Interagency Agreement DW89931336-01-6.

LBL-28072

A Semi-Analytic Study of the Regional Flow Patterns around a Well or an Underground Drift with Complex Skin Effects.

Pascal Bidaux[*] *and Chin-Fu Tsang*

Earth Sciences Division, Lawrence Berkeley Laboratory,
1 Cyclotron Road, Berkeley, CA 94720

[*]Permanent address:
CNRS - Laboratoire d'Hydrogéologie, Université des Sciences et Techniques,
Pl. E. Bataillon, 34060 Montpellier Cedex, France

ABSTRACT

A semi-analytic solution is given for steady-state flow around a wellbore or a drift with a complex skin, in which the hydraulic conductivity may continuously vary as a function of the radial distance from the well (or drift), and even be radially anisotropic. Such configurations can be found around damaged or acidized wellbores or around a drift near which the stress redistribution induces radial anisotropy. Purely radial flow, regional flow around an open or cemented hole without pumping or injecting, and combined regional and radial flow are considered. Variations of hydraulic potential and Darcy velocity in various radial directions are studied for several cases. It is shown that the convergence of the streamlines toward the hole, the hydraulic potential, and the Darcy velocity fields are strongly affected by a complex skin. This should be taken into account in applications involving the point dilution method of measuring regional flow velocity and in some applications involving single-well capture zone analysis. Also, a number of recent field experiments have been carried out in underground drifts in fractured rocks. These often involve pressure and tracer tests in boreholes drilled radially from the drift. Analysis of these tests should include the effects of regional head and velocity distribution around the drift, such as those calculated by our model.

1. INTRODUCTION

Determining the groundwater flow in an aquifer around a wellbore (or a cylindrical drift) with a radially varying hydraulic conductivity (damaged or developed skin) is an important problem in many applications, such as reservoir engineering, where the hydraulic conductivity around the well is often

artificially increased by acidization or hydraulic fracturing in order to improve productivity and toxic waste disposal, where the flow field near the well strongly influences wellbore data analysis methods.

Usually, the radial permeability change around a well is taken into account by introducing a skin factor that reflects, in a dimensionless form, the additional potential drop that is obtained between an infinite-distance boundary and the producing well, compared with the potential drop that would be observed in the case of a homogeneous medium. The skin factor is expressed as:

$$s = \left(\frac{K_\infty}{K_d} - 1\right) \ln \frac{R_d}{R_w} \tag{1}$$

where R_w and R_d are, respectively, the radii of the wellbore and the damaged zone, K_d and K_∞ the hydraulic conductivities of the damaged zone and the surrounding medium.

However, it seems that the skin factor, which combines the two variables R_d and K_d in one parameter, may not be suitable in all cases. For example, let us consider the regional groundwater flow around a well. The deformation of the streamlines toward the well is due to an infinitely conducting anomaly (the well), and to the presence of a skin, and this deformation causes the apparent Darcy velocity at the well to differ from the real value of the regional Darcy velocity by a multiplicative coefficient Ξ, usually called the convergence factor. This factor is essential when one intends to measure the regional flow velocity by the borehole dilution technique (Drost et al., 1968; Aubertin et al., 1987; McLinn and Palmer, 1989). But unfortunately, Ξ depends separately on K_∞/K_d and R_d/R_w, and not only on the skin factor (Bidaux and Tsang, 1989). Moreover, the model of a skin that consists of an annular region with a constant hydraulic conductivity K_d, differing from the conductivity K_∞ in the unperturbated medium, is not realistic. Mud invasion, acidization processes, and stress redistribution in the vicinity of an excavated drift (e. g., see Jaeger and Cook, 1969) suggest that the resulting perturbation of the hydraulic conductivity is, in general, radially anisotropic and reaches a maximum close to the wellbore, decreasing gradually to zero at a large distance from the wellbore.

For these reasons, we performed a general study of the groundwater flow in an aquifer around a well (or drift) with a radially varying hydraulic conductivity. The cases of regional flow without pumping, purely radial flow (pumping or injecting), and combined regional and radial flow are all studied. Given a skin configuration in terms of two functions $K_r(r)$ and $K_\theta(r)$ that describes the radial variations of the radial and tangential values of the hydraulic conductivity, the flow is determined semi-analytically by assuming radial symmetry in the configuration and performing a 1-D numerical integration with respect to the radial coordinate r. The following quantities are calculated:

- The convergence factor Ξ and the effective value of the conventional skin factor s;
- The equipotentials and streamlines;
- Radial variations of the hydraulic potential in any azimuthal direction;
- Radial variations of the absolute value of the Darcy velocity in any azimuthal direction;
- Travel times and breakthrough curves.

A computer code has been written and validated by comparing its results with the analytic solution calculated for simple expressions of $K(r)$. Examples are given and several applications are proposed, including regional flow velocity measurement and the tracer dilution problem, single-well capture zone analysis, and fluid flow and tracer transport around an underground drift.

2. THEORY

2.1 *Description of the Configuration*

We consider an isotropic aquifer of constant thickness e with a "hole" of radius R_w. The general word "hole", as used in this work may mean a wellbore, a large-diameter well, or an underground drift or tunnel. For the simple case of a developed or damaged well, we may assume that $K_r=K_\theta$, and is given by a function of radius, $K(r)$. The flow field around the well in such a system may be solved numerically, as described below. For the particular class of $K(r)$ function given by

$$\frac{K(r)}{K_\infty} = \exp\left(-\frac{u}{(r/R_w)^\gamma}\right) \tag{2}$$

where u and γ are parameters, analytic solutions may be obtained. The expressions for the skin factor and the convergence factor will be given below. For illustration, $K(r)$ for four different sets of u and γ values are shown in Figure 1*A*, and the resulting skin and convergence factors are summarized in Table 1*A*.

For a large-diameter hole, such as an underground drift, generally $K_r \neq K_\theta$. The system is radially anisotropic, and the radial variations of K_r and K_θ are of the type shown in Figure 1*B* (solid curves). Let us consider the stress redistribution due to a circular hole in a homogeneous elastic medium with a scalar stress p_0 (overburden) applied on boundaries at large distances from the hole. Then the stress field (Jaeger and Cook, 1969) is given by

$$\sigma_r = p_0\left(1 - \frac{R_w^2}{r^2}\right) \tag{3.1}$$

$$\sigma_\theta = p_0\left(1 + \frac{R_w^2}{r^2}\right) \tag{3.2}$$

$$\tau_{r\theta} = 0 \tag{3.3}$$

These expressions indicate a radial tension and tangential compression near the hole, leading probably to a simultaneous increase of the tangential permeability and decrease of the radial permeability. Models relating stress to permeability in porous or fractured media, such as those by Gangi (1978) or Tsang and Witherspoon (1981), may be used to quantify the permeability change at any point around the hole if one assumes that the principal axes of the hydraulic conductivity tensor are oriented radially and tangentially. Then changes in σ_r affect K_θ, and changes in σ_θ affect K_r. Unfortunately, these models are mainly empirical, relying on hypotheses concerning the nature of the medium, or are valid only for a narrow range of stress values. The stress-permeability relationships based on these models, however, may be used as guidelines. Laboratory experiments, such as those carried out by Holt (1989), may also provide useful data, although they involve small samples and are limited to one type of rock. As a general rule, when σ increases, K decreases asymptotically from K_0 (permeability without stress) to a minimum value K_l; increasing σ over a value σ_l has no further significant effect on permeability. Thus, the stress release in the radial direction always enhances the tangential permeability, but the tangential compression may not affect the radial permeability if the overburden stress p_0 is close to or

greater than σ_l.

The stress-induced permeability reduction can be quantified by fitting an empirical exponential negative function to the experimental values $K=f(\sigma)$. Such job has been performed on data for Red Wildmoor sandstone (Holt, 1989). Although a sharper decrease in permeability is observed at high stress values, the fitting has a broad range of validity, up to 70 MPa (Figure 2). Like for the present example at low stress values, the permeability of the radially anisotropic configurations that we chose to study is assumed to vary exponentially as a function of stress, which is a simple but reasonable choice. For any stress value σ, the hydraulic conductivity K is given by

$$K(\sigma) = K_l + (K_0 - K_l)\left(\frac{K_\infty - K_l}{K_0 - K_l}\right)^{\sigma/p_0} \tag{4}$$

where K_0, K_∞, and K_l are the hydraulic conductivity values for $\sigma=0$, $\sigma=p_0$, and $\sigma=\infty$, respectively. The variations of K_r and K_θ as a function of r are obtained by combining (3) and (4):

$$K_r(r) = K(\sigma_\theta) = K_l + (K_0 - K_l)\left(\frac{K_\infty - K_l}{K_0 - K_l}\right)^{(1+R_w^2/r^2)} \tag{4.1}$$

$$K_\theta(r) = K(\sigma_r) = K_l + (K_0 - K_l)\left(\frac{K_\infty - K_l}{K_0 - K_l}\right)^{(1-R_w^2/r^2)} \tag{4.2}$$

Note that in the case $K_l=0$, wherein the rock becomes impermeable under very high stress values, these expressions are of the same type as (2), with $\gamma=2$, $u=\pm\ln(K_0/K_\infty)$ and $\sqrt{K_r K_\theta}=K_\infty$=constant. On a logarithmic scale, the curves $K_r(r)$ and $K_\theta(r)$ would be symmetric relative to the axis $K=K_\infty$. However, the broken parts of curves for K_r and K_θ in Figure 1*B*, describing the stress effect, are not exactly symmetric, because we assume a small but finite residual permeability at high stress values ($K_l \neq 0$), which is more consistent with the experimental data.

The stress effect, which varies as R_w^2/r^2, is significant within a distance of several times the radius R_w of the hole. Besides the stress effect discussed here, a sharp increase of both radial and tangential permeability is believed to occur within a few inches of the well due to a permanent inelastic deformation caused by excavation. This increase may be modeled by multiplying both K_r and K_θ by an exponential term of the type (2), with $u>0$ and γ large enough (e. g., about 20) to have a reasonable value of penetration length. That exponential term is based neither on theoretical considerations nor on experimental measurements. However, it is qualitatively consistent with the permeability increase due to inelastic deformation effects. The curve for $K_r=K_\theta$ in Figure 1*B* shows these effects, and the solid curves show the resulting variations of K_r and K_θ due to combined stress and inelastic deformation effects. This last case is probably the most realistic, and leads to the expressions finally assumed in the examples given throughout the paper:

$$K_r(r) = \left[K_l + (K_0 - K_l)\left(\frac{K_\infty - K_l}{K_0 - K_l}\right)^{(1+R_w^2/r^2)}\right] \exp\left(-\frac{u}{(r/R_w)^\gamma}\right) \tag{4.3}$$

$$K_\theta(r) = \left[K_l + (K_0 - K_l)\left(\frac{K_\infty - K_l}{K_0 - K_l}\right)^{(1-R_w^2/r^2)}\right] \exp\left(-\frac{u}{(r/R_w)^\gamma}\right) \tag{4.4}$$

The computed values of the skin factor and the convergence factor in all the cases considered (with or without stress effect, and with or without inelastic deformation effect) are given in Table 1*B*.

2.2 *Flow Equations and Studied Flow Types*

The flow in all cases studied is assumed to be steady state, two dimensional, incompressible, and to obey Darcy's law. Thus the flow equations are Darcy's law and the incompressibility condition:

$$\vec{V} = \bar{\bar{K}}\,\vec{\nabla}\phi \tag{5}$$

$$\nabla\vec{V} = 0 \tag{6}$$

where ϕ is the hydraulic potential and $\vec{V}$, the Darcy velocity. ϕ obeys the diffusivity equation which is obtained by eliminating $\vec{V}$ between equations (5) and (6). In the present study, we use a method inspired from the complex potential theory rather than the diffusivity equation. As pointed out by Hubbert (1940), no velocity potential (i. e., a function ϕ_V verifying $\vec{V} = \vec{\nabla}\phi_V$) exists when the medium is heterogeneous. Therefore, it is not possible to use the complex potential theory in a strict sense. However, the problem can still be solved using a stream function ψ whose formulation implies that the incompressibility condition is satisfied. In cylindrical coordinates, (5) can be written as

$$V_r = -K_r\frac{\partial\phi}{\partial r} \tag{5.1}$$

$$V_\theta = -\frac{K_\theta}{r}\frac{\partial\phi}{\partial\theta} \tag{5.2}$$

and (6) is satisfied if ψ verifies the following equations:

$$V_r = -\frac{1}{r}\frac{\partial\psi}{\partial\theta} \tag{6.1}$$

$$V_\theta = \frac{\partial\psi}{\partial r} \tag{6.2}$$

in which case the equation of a streamline is ψ = constant. For any set of boundary conditions, the flow can be calculated using the equations (5.1), (5.2), (6.1), and (6.2).

The flow types considered in the present paper correspond to different boundary conditions at the hole or at large distances from the hole. We may have a production Q at the hole ($Q>0$ for pumping, $Q<0$ for injecting), a regional flow (Darcy velocity V_∞, apparent velocity at the hole $V_w = \Xi V_\infty$), or the superposition of both production and regional flow. The production may correspond to intentional pumping/injecting in a wellbore, or to the flow into a non-cemented underground drift, which is kept dry by pumping/draining. The boundary conditions at the hole are equipotential in the general case, or impermeable for the case of regional flow around a cemented tunnel. The various combinations are summarized in Figure 3, in which they are referred to as flow types 1 through 4. A detailed study of each is provided below.

2.3 *Purely Radial Flow (Pumping/Injection), Flow Type* 1

As we have radial symmetry for all the variables, the Darcy velocity $\vec{V}$ is purely radial, and its algebraic value V (positive axis oriented outward from the hole) is simply given by flux conservation, independent of the variations of K:

$$V_r(r) = -\frac{Q}{2\pi e r} \tag{7}$$

The hydraulic potential field ϕ satisfies Darcy's law:

$$-K_r \frac{d\phi}{dr} = V_r(r) = -\frac{Q}{2\pi e r}$$

which yields

$$\phi(r) = \frac{Q}{2\pi e} \int_{R_w}^{r} \frac{d\rho}{\rho K_r(\rho)} \tag{8}$$

with the convention $\phi=0$ at the hole where $r=R_w$. In order to estimate the skin factor in that configuration, (8) has to be compared with the expression of the hydraulic potential for a homogeneous medium of constant conductivity K_∞:

$$\phi_0(r) = \frac{Q}{2\pi K_\infty e} \ln\frac{r}{R_w} = \frac{Q}{2\pi K_\infty e} \int_{R_w}^{r} \frac{d\rho}{\rho}$$

Hence the additional potential drop due to the radial heterogeneity of hydraulic conductivity can be expressed as

$$\delta(r) = \phi(r) - \phi_0(r) = \frac{Q}{2\pi K_\infty e} \int_{R_w}^{r} \left(\frac{K_\infty}{K_r(\rho)} - 1\right) \frac{d\rho}{\rho}$$

The skin factor is the limit value of that expression when r tends to infinity, in a dimensionless form ($Q = 2\pi$, $e = 1$, $K_\infty = 1$):

$$s = \int_{R_w}^{\infty} \left(\frac{K_\infty}{K_r(\rho)} - 1\right) \frac{d\rho}{\rho} \tag{9}$$

which is the generalized form of the classical expression (1) for the case of any radial distribution of

the hydraulic conductivity.

For any radial distribution of the hydraulic conductivity, numerical integration of equation (8) is performed to give the variations of the hydraulic potential ϕ as a function of r (Figure 4). A Simpson's method with geometrically increasing radial step sizes is used in order to obtain better accuracy near the hole, where K varies more sharply. The skin factors obtained for cases a to d plotted in Figure 1*A* are about s=–2 and s=4, which seem to be reasonable values usually found in the field. As expected, the hydraulic potential near the hole is strongly smoothed in the case of a negative skin factor (case a) compared with the potential profile in a homogeneous medium. Conversely, the gradient near the hole increases more sharply in the case of a positive skin factor (cases b to d). For different cases with the same value of s, the potential profiles are the same outside of the skin. Only observation wells located inside the damaged zone, close to the main hole, could distinguish between them.

2.4 *Regional Flow Without Pumping, Flow Types* 2–3

The radial symmetry of the configuration makes it possible to reduce the problem to one dimension by separating the variables r and θ. Let us try to write the functions ϕ and ψ in the following form:

$$\phi(r,\theta) = \left[a(r)r^{\alpha(r)} + \frac{b(r)}{r^{\alpha(r)}}\right] \cos\theta \tag{10.1}$$

$$\psi(r,\theta) = \hat{K}(r)\left[a(r)r^{\alpha(r)} - \frac{b(r)}{r^{\alpha(r)}}\right] \sin\theta \tag{10.2}$$

where the following quantities have been defined:

$$\alpha(r) = \sqrt{K_\theta(r)/K_r(r)} \tag{11.1}$$

$$\hat{K}(r) = \sqrt{K_\theta(r)\,K_r(r)} \tag{11.2}$$

By calculating the partial derivatives of ϕ and ψ in (10.1) and (10.2), and by identifying the subsequent values of V_r and V_θ given, respectively, by (5.1) and (5.2) for ϕ, and by (6.1) and (6.2) for ψ, it appears that the flow equations are verified if and only if a and b obey the following differential system:

$$\begin{aligned} 2a'(r) &= \left[\frac{b(r)}{r^{2\alpha(r)}} - a(r)\right]\frac{\hat{K}'(r)}{\hat{K}(r)} - 2a(r)\,\alpha'(r)\ln r \\ 2b'(r) &= \left[r^{2\alpha(r)}a(r) - b(r)\right]\frac{\hat{K}'(r)}{\hat{K}(r)} + 2b(r)\,\alpha'(r)\ln r \end{aligned} \tag{12}$$

where the symbol $'$ is used for the derivative of a single-variable function. Hence, instead of directly calculating ϕ and ψ, it is possible to determine, in a first step, the auxiliary functions a and b which

are more convenient. This is done by solving (12), which is a first-order coupled linear differential system. It has an unique solution if the boundary conditions $a(R_w)$ and $b(R_w)$ are known. These two limiting values are given by the type of boundary conditions at the hole:

For an equipotential hole (wellbore of infinite conductivity),

$$a(R_w) = \frac{V_w}{2R_w^{\alpha(R_w)-1}\hat{K}(R_w)} \tag{13.1}$$

$$b(R_w) = -\frac{R_w^{\alpha(R_w)+1}V_w}{2\hat{K}(R_w)} \tag{13.2}$$

For an impermeable hole (cemented tunnel),

$$a(R_w) = \frac{i_w}{2R_w^{\alpha(R_w)-1}} \tag{14.1}$$

$$b(R_w) = \frac{R_w^{\alpha(R_w)+1}i_w}{2} \tag{14.2}$$

To solve equations (12) with a set of boundary conditions (13) or (14), the apparent velocity V_w or the apparent hydraulic gradient i_w at the hole can be taken arbitrarily as a parameter and then adjusted so that the solution at an infinite distance from the hole corresponds to the uniform flow in the homogeneous aquifer ($a_\infty = i_\infty = V_\infty/K_\infty$).

Once the integration of a and b has been performed, the flow problem is completely solved. ϕ and ψ are respectively given by (10.1) and (10.2), and $\vec{V}$ by either ((5.1),(5.2)) or ((6.1),(6.2)), which can also be written in the following equivalent form:

$$V_r(r,\theta) = -\hat{K}(r)\left[a(r)\,r^{\alpha(r)-1} - \frac{b(r)}{r^{\alpha(r)+1}}\right]\cos\theta \tag{15.1}$$

$$V_\theta(r,\theta) = \alpha(r)\,\hat{K}(r)\left[a(r)r^{\alpha(r)-1} + \frac{b(r)}{r^{\alpha(r)+1}}\right]\sin\theta \tag{15.2}$$

Equations (10.1) and (15) provide an explicit form for the potential field and the Darcy velocity field, which can be easily calculated for any point of the aquifer. The plotting of equipotentials and streamlines requires the solution of polar equations $\phi(r,\theta)=\phi_0$ or $\psi(r,\theta)=\psi_0$, which is simply done by calculating θ as a function of r. The convergence factor is then given by the expression

$$\Xi = \frac{V_w}{V_\infty} = \frac{V_w}{K_\infty a_\infty} \tag{16}$$

As expected, for a homogeneous medium ($K_r(r)=K_\theta(r)=K_\infty$=constant), system (12) gives $a'(r)=0$ and $b'(r)=0$, so that a and b keep their boundary value everywhere. For an equipotential hole, we get $\Xi=2$.

Our calculation generalizes the classical result of the thermal problem of a cylinder of conductivity K_1 in a matrix of conductivity K_2 (Carslaw and Jaeger, 1959).

The differential system (12) can also be solved for any given coupled functions (K_r, K_θ), which may be derived from the stress redistribution around the hole. First, K_r and K_θ are replaced by their dual functions $\hat{K}$ and α. Then, starting at the hole ($r=R_w$), the medium is discretized in n points, with the same geometrically increasing radial step size as in the purely radial flow, and the arrays for r, $\hat{K}$, and α are created:

$$r_1 = R_w$$
$$r_{i+1} = r_i \beta \qquad (\beta>1)$$
$$\hat{K}_i = \hat{K}(\sqrt{r_i r_{i+1}})$$
$$\alpha_i = \alpha(\sqrt{r_i r_{i+1}})$$

Based on the following approximations for the derivatives:

$$\alpha'(r) \ln r \, \Delta r = r^{\alpha(r+\Delta r)-\alpha(r)} - 1 + o(\Delta r)$$
$$f'(r) \Delta r = f(r+\Delta r) - f(r) + o(\Delta r)$$

where f designates any of the functions a, b or $\hat{K}$, and after dropping the terms of a higher order than Δr, the differential system (12) is discretized using the following scheme:

$$2a_{i+1} = a_i r_i^{\alpha_i-\alpha_{i+1}} \left[1+\frac{\hat{K}_i}{\hat{K}_{i+1}}\right] + \frac{b_i}{r_i^{\alpha_i+\alpha_{i+1}}} \left[1-\frac{\hat{K}_i}{\hat{K}_{i+1}}\right]$$
$$2b_{i+1} = a_i r_i^{\alpha_i+\alpha_{i+1}} \left[1-\frac{\hat{K}_i}{\hat{K}_{i+1}}\right] + \frac{b_i}{r_i^{\alpha_i-\alpha_{i+1}}} \left[1+\frac{\hat{K}_i}{\hat{K}_{i+1}}\right] \qquad (17)$$

which generalize the recurring expressions given by J. Goguel in an unpublished note written in 1984 (courtesy of G. de Marsily) for a medium consisting of a succession of constant-conductivity concentric annuli of radii R_i, $i=1,n$ and isotropic hydraulic conductivities K_i, $i=1,n$. The values a_1 and b_1 are given by the appropriate set of boundary conditions:

For an equipotential hole,

$$a_1 = \frac{V_w}{2R_w^{\alpha_1-1}\hat{K}_1}$$
$$b_1 = -\frac{R_w^{\alpha_1+1}V_w}{2\hat{K}_1}$$

For an impermeable hole,

$$a_1 = \frac{i_w}{2R_w^{\alpha_1 - 1}}$$

$$b_1 = \frac{R_w^{\alpha_1 + 1} i_w}{2}$$

A computer code was written that performs the numerical integration of the functions a and b, calculates the convergence factor $\Xi = V_w/(K_\infty a_n)$ for the equipotential hole case, plots the flow pattern (streamlines, equipotentials), and calculates the radial variations of the hydraulic potential ϕ and the Darcy velocity V in any azimuthal direction. As an example, Figure 5 gives the flow pattern for a developed well, a damaged well, and an open or cemented tunnel with radially anisotropic stress effect. For the first two cases, equipotentials and streamlines are rectangular (isotropic skin) but do not form curvilinear squares as in a homogeneous medium. The two cases of flow around the tunnel show clearly that equipotentials and streamlines are no longer rectangular (anisotropic effect). These two functions do not have symmetric roles and cannot be interchanged by altering the boundary conditions, as in the case of a homogeneous isotropic medium. This is related to the fact that ϕ and ψ are not conjugate harmonic functions. Figure 6 gives the hydraulic potential profile in the direction $\theta=0$. For a wellbore, a high-permeability skin (part *A*, plot *a*) flattens the starting of the profile, and a low-permeability skin (part *A*, plot *b*) sharpens it. For a drift without stress effect (part *B*, dashed line), the profile near the drift changes significantly whether the drift is open or cemented. With stress effect (part *B*, solid line), the potential profile is much less affected by the boundary conditions at the drift wall. This is because the flow tends to go around the hole independently of the boundary conditions, in response to an enhanced tangential permeability near the drift. Thus the drift is nearly equipotential, even if it is cemented. The Darcy velocity profiles in three azimuthal directions, for an open drift (Figure 7*A*), shows that the stress effect modifies Darcy velocity even though the hydraulic potential is not affected (see Figure 6*B*). For a cemented drift (Figure 7*B*), the flow is highly concentrated in the high-permeability ring close to the drift. The stress effect, which increases tangential permeability near the drift with the result that the flow there is approximately tangent, enhances that flow concentration and reduces the size of the zone in which the flow is perturbed.

2.5 *Regional Flow with Pumping, Flow Type* 4

This is simply the superposition of cases 1 and 2. The linearity of the flow equations gives the expressions for the hydraulic potential and the stream function:

$$\phi(r,\theta) = \left[a(r)\, r^{\alpha(r)} + \frac{b(r)}{r^{\alpha(r)}}\right] \cos\theta + \frac{Q}{2\pi e} \int_{R_w}^{r} \frac{d\rho}{\rho K_r(\rho)} \tag{18.1}$$

$$\psi(r,\theta) = \hat{K}(r) \left[a(r)\, r^{\alpha(r)} - \frac{b(r)}{r^{\alpha(r)}}\right] \sin\theta + \frac{Q}{2\pi e}\theta \tag{18.2}$$

where a and b are the functions determined in the preceding section, with the boundary conditions

corresponding to an equipotential hole. The Darcy velocity is given by the following expressions:

$$V_r(r,\theta) = -\hat{K}(r)\left[a(r)r^{\alpha(r)-1} - \frac{b(r)}{r^{\alpha(r)+1}}\right]\cos\theta - \frac{Q}{2\pi er} \tag{19.1}$$

$$V_\theta(r,\theta) = \alpha(r)\,\hat{K}(r)\left[a(r)r^{\alpha(r)-1} + \frac{b(r)}{r^{\alpha(r)+1}}\right]\sin\theta \tag{19.2}$$

Equation (19.2) is identical to (15.2), as the production does not change the tangential component of flow velocity.

Thus, as in the case of regional flow without pumping, the equipotentials and streamlines and the hydraulic potential and Darcy velocity azimuthal profiles can be easily plotted once the integration of the functions a and b has been performed. Moreover, a and b, which depend only on the functions K_r, K_θ, can be calculated and stored for the study of the regional flow alone and for productions at various flow rates.

The shapes of the streamlines deserves particular attention. The equation of a streamline is

$$\hat{K}(r)\left[a(r)\,r^{\alpha(r)} - \frac{b(r)}{r^{\alpha(r)}}\right]\sin\theta + \frac{Q}{2\pi e}\theta = \text{constant}$$

For a given value of r, θ is given by solving a transcendental equation of the type

$$\sin\theta + \lambda\theta = \mu$$

With the condition $0\le\theta\le\pi$, for appropriate values of μ, the equation has two roots if $|\lambda|<1$ and only one root if $|\lambda|>1$; and for $|\lambda|=1$, $\theta=0$ and $\theta=\pi$ may be the double root. The streamline ($\psi=\psi_0$) reaches the hole ($r=R_w$) with an angular coordinate θ satisfying the equation

$$R_w V_w \sin\theta + \frac{Q}{2\pi e}\theta = \psi_0 \tag{20}$$

Thus the flow pattern at the hole is different depending on whether we have $|q|<1$ or $|q|>1$, where q is the dimensionless pumping or injection rate defined by

$$q = \frac{Q}{Q_c}$$

$$Q_c = 2\pi e R_w V_w$$

We call Q_c the critical value of flow rate. At a supercritical flow rate ($|q|>1$), equation (20) has at most one root: all the water arriving at the borehole is produced, or for injection case, all the water entering the formation is injected water. At a subcritical flow rate ($|q|<1$), equation (20) has two roots for appropriate values of ψ_0, which means that a given streamline may represent flow into and out of the hole. For the case of injection, the flow leaving the hole and entering the formation is a

combination of injected fluid and fluid from the formation upstream. For the case of pumping, only part of the flow from the formation upstream is produced; the rest re-enters the formation downstream. A similar result has been obtained in the case of classical skin configurations (Bidaux and Tsang, 1989; J. Goguel, unpublished manuscript, 1984).

At a supercritical flow rate, there is a value r_s such that

$$\hat{K}(r_s)\left[a(r_s)\, r_s^{\alpha(r_s)} - \frac{b(r_s)}{r_s^{\alpha(r_s)}}\right] = \frac{Q}{2\pi}$$

Thus, $\theta=\pi$ is a double root of the equation

$$\hat{K}(r_s)\left[a(r_s)\, r_s^{\alpha(r_s)} - \frac{b(r_s)}{r_s^{\alpha(r_s)}}\right] \sin\theta + \frac{Q}{2\pi}\theta = \frac{Q}{2}$$

The point ($r=r_s$, $\theta=\pi$) is a stagnation point, and the singular streamline ($\psi=Q/2$) distinguishes the capture zone (Javandel and Tsang, 1986) from the rest of the aquifer. Qualitatively, this is the classical configuration obtained for a line-source well in a homogeneous isotropic aquifer.

Our formula for the critical flow rate Q_c is expressed in terms of the apparent Darcy velocity at the hole, and not the regional flow velocity. If we re-introduce the regional flow velocity and the convergence factor, we can write the complete expression of the critical value for the flow rate:

$$Q_c = 2\pi \Xi e R_w V_\infty \tag{21}$$

Since Q_c depends on the convergence factor Ξ, for given values of the regional flow velocity and the production flow rate, we may have either subcritical or supercritical flow, depending on whether the hole has a skin that is more or less conductive than the original aquifer.

Assuming an isotropic complex skin (equation (2)), the streamlines and equipotentials for the cases of subcritical, critical, and supercritical flows are plotted in Figure 8. It appears that for a given value of regional flow V_∞, hydraulic conductivity K_∞, thickness e, hole radius R_w, and pumping rate Q, the flow may be either sub- or supercritical, whether the skin is more or less conductive. For example, in Figure 8, the subcritical flow in the developed configuration a (top, left) and the supercritical flow in the damaged configuration b (right, bottom) correspond to about the same value of pumping rate. The less the convergence factor, the more likely a supercritical flow will be obtained.

Figure 9 gives hydraulic potential profiles in which five types of curves can be distinguished: linear increase of ϕ (curve 1), logarithmic increase (curve 2) for the flow line perpendicular to the regional flow direction, increase and then decrease (curve 3), and monotonous decrease with or without vanishing derivative at the entry of the hole (curves 4 and 5). As in the cases of radial flow alone or regional flow alone, the gradient near the hole is smaller for a negative skin factor and larger for a positive one.

Type curves for Darcy velocity profiles are not so easy to define. To get the expression of V at a large distance from the hole, one should first find asymptotic expressions for a and b, which are not simply related to K_r and K_θ. This development does not seem worth pursuing in practical cases, because the velocity field far from the hole is probably more affected by other external perturbations than by the complex skin. At the hole ($r=R_w$), the following expressions for V_r and V_θ may be useful:

$$V_r \approx \left(-V_w \cos\theta - \frac{Q}{2\pi e R_w}\right)\left(1 - \frac{r-R_w}{R_w}\right)$$

$$V_\theta \approx \left[\alpha(R_w)\frac{V_w}{R_w}\sin\theta\right]\frac{r-R_w}{R_w}$$

Hence the following patterns can be distinguished at $r=R_w$:

General case: $V\neq 0$ and $\partial V/\partial r < 0$.

Case $V=0$ and $\partial V/\partial r > 0$ (singular point for a subcritical flow).

Case $V=0$ and $\partial V/\partial r = 0$ (singular point for a critical flow).

In the general case, V may monotonously decrease to V_∞ or decrease to a minimum value and then increase to reach V_∞. For $\theta=\pi$ in a supercritical flow condition, the minimum value of V is 0 (stagnation point). But in the case of a low-conductivity skin, two or even three extrema may be observed. The reason for this is that, even though the less conductive skin has no influence on the radial flow velocity, it strongly reduces the regional flow velocity in the vicinity of the well. In some cases, the first minimum may be so close to the hole that it does not appear visually, resulting in an apparent velocity increase at $r=R_w$, which has been shown to be impossible theoretically. Hence a large variety of curve types can be found for the velocity profiles, considering the behavior at the well and the possibility of having a stagnation point and a number of extrema. Several examples are given in Figure 10.

3. APPLICATIONS

3.1 *Regional Flow Velocity Measurement and Tracer Dilution Problem*

This section addresses the effect of a complex skin on the convergence factor Ξ and discusses the possible values of Ξ that may correspond to a given skin factor s.

The convergence factor is essential for the borehole dilution technique, a classical method of measuring regional flow velocity in an aquifer (Drost et al., 1968) and one that is still subject to recent improvements (McLinn and Palmer, 1989). The apparent velocity V_w at the borehole is estimated by observing the dilution rate of a tracer, and the regional Darcy velocity is then given by $V_\infty=V_w/\Xi$. The value $\Xi=2$, corresponding to the result for a homogeneous medium, is generally used, although a higher value should be better for the case of an acidized well (Aubertin at al., 1987). Bidaux and Tsang (1989) carried out a more extensive study of the influence of a conventional skin (outer radius R_d, constant hydraulic conductivity K_d) on the convergence factor. The case of a complex skin is examined below.

The hydraulic conductivity K is considered to be isotropic at any point and given by function (2). The exponential decrease of the permeability perturbation may describe the damage caused by mud invasion or the well development performed by acidization. As no data concerning the permeability change around a well are available, this function cannot be justified rigorously. It is chosen for its mathematical convenience to give a fully analytic solution, which can then be used to validate the numerical model for any other specified skin model. Function (2) reflects a permeability perturbation that is maximum close to the well and becomes smaller more or less rapidly with distance from the well. A positive value of u means a permeability decrease near the well (damage), and a negative value indicates that the well is developed. As the hydraulic conductivity at the well is $K(R_w)=\exp(-u)$, the absolute value of u gives the magnitude, on a logarithmic scale, of the permeability change close to the well. The parameter γ can be interpreted in terms of thickness of the damaged or developed zone or skin: the lower the value of γ, the thicker the skin. Let us define a penetration radius R_p of the skin by

$$\frac{\ln K(R_p)}{\ln K(R_w)} = \frac{1}{e}$$

We then get

$$R_p = \exp(\frac{1}{\gamma})$$

Using equation (4), the skin factor is given by the expression

$$s = \int_{R_w}^{\infty} (e^{-\frac{u}{(r/R_w)^\gamma}} - 1)\frac{dr}{r} = \frac{1}{\gamma}\int_0^u (e^x - 1)\frac{dx}{x} \qquad (22)$$

and a fully analytic solution for the system of differential equations (9) and (10) can be provided for most fractional values of γ. An explicit form of the convergence factor may then be obtained:

$$\Xi = \frac{2}{\sum_{n=0}^{\infty} \eta_{\gamma,n} u^n} \qquad (23)$$

where the coefficients $\eta_{\gamma,n}$ can be calculated by the recurrence formulae

$$\eta_{\gamma,0} = 1 \quad , \quad \eta_{\gamma,n} = \frac{\frac{1}{\gamma}+n-1}{n(\frac{2}{\gamma}+n)}\,\eta_{\gamma,n-1}$$

For some values of s, the variations of Ξ as a function of the dimensionless penetration radius of the skin R_p/R_w-1 have been plotted (Figure 11*A*) and the results compared with those obtained using the conventional model of skin (Figure 11*B*). Qualitatively, we observe in both cases that for a given value of s, the convergence factor tends to its limiting value Ξ=2 with increasing skin thickness. For damaged wells, the limiting value of Ξ for an infinitely thin damaged zone of infinitely low permeability is $1/(1+s)$ in both cases. The main difference is observed for developed wells. With the classical model, the maximum convergence factor is 4 for any negative value of s. But the present model can yield, for reasonable values of s, convergence factors exceeding 10. This is because the refraction of the streamlines is due to permeability gradients and not to high permeability values. In the classical model, only two refractions are obtained (entering the developed zone and entering the well), giving a maximum value of 4 for the convergence factor. With a continuously varying hydraulic conductivity, the streamlines are refracted all along their path from a large distance to the well. On the other hand, one notes that for negative skin factors corresponding to large developed zones with a low permeability contrast, both conventional and complex skins still give comparable results. In Figure 11, the two graphs, except for the portions corresponding to abnormally high convergence factors for complex skins, can be superimposed with a shift of 2 along the thickness axis. Thus a complex skin, described by the present model, with a penetration radius R_p and corresponding to a skin factor s, behaves in most cases like a conventional skin of thickness

$$R_d - R_w = 2\,(R_p - R_w)$$

But abnormally high values of convergence factor can also be obtained for complex skins in the negative s cases, where there is a large permeability contrast and a rather shallow penetration radius.

Thus, when using the borehole dilution technique, very high values of the convergence factor should be assumed in the case of a negative skin factor. Investigations should be made to obtain an idea of the radial distribution of hydraulic conductivity; otherwise, the uncertainty of the derived value for the regional flow may be as much as one order of magnitude.

Another problem addressed in Bidaux and Tsang (1989) is the tracer dilution in water injected into the formation. If a tracer is injected in a wellbore at a subcritical flow rate, the flow leaving the well and entering the formation is a mixture of injected fluid and water from the formation upstream. The effective concentration entering the formation can be calculated as a function of the injection flow rate (Figure 12), and depends only on the critical value Q_c of flow rate. Thus the same expression is still valid for a complex skin if Q_c is given by (18). But much higher values of Q_c may be obtained compared with the case of a conventional skin, since Ξ may be very large in some cases. These considerations may be of importance in the analysis of tracer tests where tracer is injected at a low flow rate to avoid changing the original flow field.

3.2 *Single-Well Capture Zone Analysis*

Aquifer cleanup operations often require determination of the capture zone of a well. Javandel and Tsang (1986) proposed an analysis based on the assumption that the well is a line-sink, and that the aquifer is a homogeneous medium (no skin effects). We investigate the influence of a wellbore skin on the capture zone by studying the effect of the skin on the distance r_s between the pumping well and the

stagnation point caused by the interaction of radial flow and regional flow.

The first part of our study was done using the conventional skin model for reasonable values of pumping rate, say, $Q/(eR_wV_\infty) = 10^3$ or 10^4. Without a skin, the distance between the stagnation point and the well is

$$r_s \simeq r_{s_0} = \frac{Q}{2\pi eV_\infty}$$

where the finite wellbore effect is neglected, since $R_w \ll r_{s_0}$. With a skin, the influence on the capture zone appears to be significant only if R_d is at least about the same order of magnitude as r_{s_0} (Figure 13*A*–*B*). The capture zone is smaller ($r_s < r_{s_0}$) for $s<0$ and larger for $s>0$.

In practical cases, it is extremely rare to have large wellbore skins, although ratios up to $R_d/R_w=200$ have been assumed in acidized geothermal wells with highly negative skin factors (De Marsily, 1984, personal communication). Thus, except in such situations, the capture zone remains unchanged when there is a wellbore skin.

Another point should be mentioned about large wellbore "skins." If a borehole is located in a zone of higher or lower conductivity than that of the whole aquifer, that zone may behave like a huge "natural skin" and the capture zone may be modified. For example, with $Q/(eR_wV_\infty) = 10^4$ and $R_w = 0.1$ m, the stagnation point, which would be located at a distance $r_{s_0} = 159$ m from the well without heterogeneity, might be displaced about 45 m toward the well (Figure 13*B*) in some cases. This is a much smaller capture zone than expected, which should be taken into account when designing an aquifer cleanup operation.

In the case of a complex skin, in which the radial permeability distribution is given by (2), the results (Figure 13*C*–*D*) are qualitatively comparable with those for a conventional skin. For given values of pumping rate and positive skin factor, the stagnation point moves away and then comes back to its original location as the penetration radius R_p increases. For a negative skin factor, it moves first toward the well and then back to its original location. However, the curves describing variations of the stagnation point displacement as a function of the skin penetration radius are smoother than the corresponding curves for a conventional skin, since no permeability discontinuity exists between the skin and the rest of the aquifer. Moreover, the maximum values of stagnation point displacement are much smaller than for a conventional skin. Thus, if the purpose of the analysis is just to estimate the minimum extension of the capture zone, a study based on the conventional model would provide the most pessimistic case and should be sufficient. On the other hand, contrary to the case of a conventional skin, non-negligible stagnation point displacements can be observed even if the penetration radius R_p is much smaller than the theoretical distance r_{s_0} between the well and the original stagnation point. This is because, for a complex skin, the permeability is in fact perturbed much beyond the distance R_p.

3.3 *Study of the Flow Around an Underground Drift*

The calculations discussed in the previous section are also useful to the understanding and analysis of the flow and hydraulic potential distribution around an underground drift by means of observation boreholes drilled radially from the drift. Such measurements were made by Wilson et al. (1981) and Neretnieks (1987) at Stripa, and by Cacas et al. (1987a-b) at Fanay-Augères. Figure 14*A* shows the arrangement in the Fanay-Augères drift.

The radial flow into an isolated drift is caused by the head difference between the water table and the drift, which is maintained at atmospheric pressure. The drift is kept dry by pumping away water that flows into the drift. If the drift of radius R_w is located at depth h below the water table, with $h>>R_w$, the flow to the drift is approximately radial and the flow rate has the following value:

$$Q = \frac{2\pi K_\infty e h}{\ln\frac{2h}{R_w} + s}$$

A regional flow gradient i_∞ may be superposed upon the radial flow to the drift. In section 2.4 on the case of combined radial and regional flow, a critical value of flow rate Q_c is defined that discriminates three types of flow. Using expression (21) for Q_c, we get

$$\frac{Q}{Q_c} = \frac{h}{R_w i_\infty \Xi(\ln\frac{2h}{R_w} + s)}$$

Thus it appears that for ordinary values of hydraulic gradient (i_∞ on the order of 10^{-3}), Q/Q_c is very large (on the order of 10^3), and the regional flow can be neglected compared with the radial flow to the drift. However, in heterogeneous media or in the presence of hydraulic boundaries or neighboring drifts, it is possible to have a local increase of the hydraulic gradient at the drift under study. Such local high values of "pseudo-regional" flow around a studied drift are observed at Fanay-Augères (Figure 14*B*), and the cause is suspected to be the presence of a neighboring drift. If a second drift of radius R_w' is located at depth h' below the drift under study, a rough estimate of the flow perturbation induced at the studied drift can be simply made. Neglecting the perturbation caused by the studied drift, the flow rate to the second drift, due to gravity, is

$$Q' = \frac{2\pi K_\infty e h'}{\ln\frac{2h'}{R_w'} + s'}$$

and if $h-h'$ is large compared to R_w, the gravity flow to the second drift induces roughly parallel hydraulic potential contours in a small region around the studied drift. The Darcy velocity of that pseudo-uniform flow is

$$V_\infty' = \frac{Q'}{2\pi e\,(h'-h)} = \frac{K_\infty h'}{(h-h')\,(\ln\frac{2h'}{R_w'} + s')}$$

For that pseudo-regional flow, the critical flow rate for the studied drift is

$$Q_c' = \frac{2\pi\Xi K_\infty e R_w h'}{(h-h')\left(\ln\frac{2h'}{R_w'} + s'\right)}$$

and we have

$$\frac{Q}{Q_c'} = \frac{h\,(h'-h)}{\Xi R_w h'} \frac{\ln\frac{2h'}{R_w'} + s'}{\ln\frac{2h}{R_w} + s}$$

The enhanced apparent value of the regional hydraulic gradient around the studied drift is

$$i_\infty' = \frac{h'}{(h-h')\left(\ln\frac{2h'}{R_w'} + s'\right)}$$

which can approach 1 for reasonable configurations ($i_\infty' = 0.47$ for $h = 200$ m, $h' = 300$ m, $R_w' = 1$ m, $s' = 0$). The combined radial and pseudo-regional flow, although supercritical, may be sufficiently asymmetrical ($Q/Q_c' \approx 10$) to have the stagnation point rather close to the drift (about 10 m). Thus the radial variations of hydraulic potential, measured between packers in observation wells, should not be expected to be given by the simple case of radial flow (Figure 4), but may be similar to those plotted in Figure 9 (flow type 4, supercritical case). It is important to know these hydraulic potential variations so that we do not misinterpret field data that show a deviation from the simple radial hydraulic variation.

The values of flow rates and hydraulic gradients given above are only very rough estimates, because the problem of the interference between two drifts would require a more rigorous calculation which can only be done numerically. Even the flow to an isolated drift in a homogeneous medium does not have a simple analytic solution when the approximation $R_w << h$ is not valid, because the drift cannot be considered as equipotential. But such studies are beyond the scope of the present paper; the results given here should be considered only as suggestions that such flow patterns around underground drifts are possible, and therefore great care should be taken in data analysis to avoid attributing such patterns to other unrelated effects.

3.4 *Tracer Emergence into an Underground Drift*

Another application of the present study is the calculation of travel time and the simulation of tracer test from the radial boreholes into the drift. If a tracer is released at a point M_0 of polar coordinates (r_0,θ_0), the stream function ψ_0 at M_0 can be calculated using (18.2), and the value obtained indicates the streamline on which M_0 is located. If dispersion is neglected, the tracer would follow exactly the path of the streamline. For a supercritical flow, two cases can be distinguished: (1) if the release point is outside the capture zone ($\psi_0 \geq Q/2e$), the tracer never reaches the drift, and (2) if the release

point is inside, the purely convective travel time to the drift can be calculated by an integration along the streamline path:

$$t_c = \int_{r=R_w}^{r=r_0} \frac{\omega(r)\,dl}{V(r,\theta(r))} \tag{24}$$

where $\theta(r)$ is given by the equation of the streamline,

$$\psi(r,\theta(r)) = \psi_0$$

dl is the elementary length along the streamline,

$$dl = \sqrt{1 + r^2(\frac{d\theta}{dr})^2}\,dr$$

$\omega(r)$ describes the radial variations of the kinematic porosity, which can be taken as either constant or radially varying, and V is the Darcy velocity, which is obtained from equations (19.1) and (19.2).

The convective travel times are calculated for various distances from the release point to the drift wall and for different values of orientation relative to the direction of the regional flow. The travel time tends to be infinitely long when the release point approaches the critical streamline delineating the capture zone, and, as expected, for a given distance within the capture zone, the travel time is longer if the tracer is injected downstream relative to the drift for the regional flow. It is interesting to consider the ratio of the travel times from two points located symmetrically on opposite sides of the drift as a function of distance for various orientations. That ratio is higher when the segment joining the two points makes a smaller angle with the regional flow direction and, for any orientation, increases sharply when one of the points approaches the critical capture zone streamline.

As we are able to compute the travel time from any point to the drift, more complex transport problems can also be studied, such as the inclusion of longitudinal dispersion along each streamline:

$$D = \alpha_L \langle V_p \rangle$$

where α_L is the longitudinal dispersivity (constant throughout the medium) and $\langle V_p \rangle = l/t_c$ is the mean pore velocity along the stream tube (l is the total length of the path). A simple computer program has been prepared to perform this calculation.

The tracer breakthrough curve along each streamtube is given by an approximate theoretical expression for a Dirac delta injection of a conservative tracer of mass m in a tube of length l, where the pore velocity $\langle V_p \rangle$ is constant:

$$C(t) = \frac{m}{\sqrt{4\pi\alpha_L \langle V_p \rangle t}} \exp\left(-\frac{(l-\langle V_p \rangle t)^2}{4\alpha_L \langle V_p \rangle t}\right) \tag{25}$$

Practically, the tracer is injected in a region of finite spatial extent. This results in additional kinematic dispersion, since the tracer particles follow their own distinct streamlines, and have different convective travel times to the drift. For n tracer particles released over the injection interval, each particle gives a response according to equation (25) and the total breakthrough curve is obtained by a superposition of these responses weighted by the corresponding fluxes:

$$C(t) = \frac{\sum_{i=1}^{n} \langle V_p \rangle_i \, C_i(t)}{\sum_{i=1}^{n} \langle V_p \rangle_i} \tag{26}$$

where each $C_i(t)$ is given by (25) with elementary mass injection,

$$m_i = C_0 \, d\Omega_i$$

where C_0 is the injected tracer concentration in the release domain and $d\Omega_i$ the elementary volume of the discretized release domain.

Let us consider a case of practical interest, in which the tracer is injected between two packers located at distances R_1 and R_2 from the drift axis ($R_1<R_2$) in a borehole drilled radially from the drift. Similar field experiments have been carried out, for example at Fanay-Augères (Cacas et al., 1987a, b). The borehole makes an angle θ with the direction of the regional flow. Two cases can be distinguished on the basis of the location of the release segment relative to the capture zone.

(1) If it is located completely inside the capture zone, the convective travel times are all between the values t_1 (for R_1) and t_2 (for R_2). The tracer breakthrough is concentrated mainly between t_1 and t_2, but longitudinal dispersion smoothes the curve and introduces both earlier and later arrivals (Figure 15*A*). Tracer recovery is 100%.

(2) If the release segment extends beyond the capture zone, some tracer particles never reach the drift (partial recovery) and others, located inside the capture zone but close to the singular streamline, have extremely long travel times. Thus the purely convective travel time starts at t_1 but has no upper limit, and the tracer breakthrough curve has a very long tail. Longitudinal dispersion smoothes the early arrival part of the curve (Figure 15*B*) but does not have much effect on the later part, for which kinematic dispersion is caused mainly by convective travel time differences from one streamline to another.

The simulated tracer breakthrough curves in Figure 15 concern a homogeneous and isotropic aquifer with no skin around the drift. Similar calculations can be performed with any type of skin. Qualitatively, it is expected that a configuration with radially isotropic or anisotropic permeability change around the drift would give a similar result because the flow is mainly radial in the vicinity of the drift, as the Darcy velocity near the drift is controlled by the flow rate to the drift rather than by permeability. Note that the effect of porosity change near the drift has not been studied but could modify the recovery curves. The patterns obtained in Figure 15 should be borne in mind in the analysis of tracer breakthrough at the drift from radial boreholes, so that such behaviors are not attributed to other unrelated effects.

4. CONCLUSION AND PERSPECTIVES

The present study has discussed the classical notion of skin and extended it to the more general case of a heterogeneous and radially anisotropic region around a wellbore or a drift. Purely radial flow, regional flow without pumping, and combined radial and regional flow have been considered. Taking advantage of the cylindrical symmetry that is assumed in the configuration, the steady-state flow problem can be analytically reduced to one dimension and solved for any radial distribution of anisotropic hydraulic conductivity by numerically integrating a linear system of two coupled first-order differential equations. A computer code has been written to calculate the hydraulic potential and Darcy velocity fields, plot the streamlines and equipotentials, and perform travel time calculations and tracer test simulations. This is a flexible tool that can be used for a number of applications.

In order to optimize the accuracy of measuring regional flow velocity by the borehole dilution technique, the effect of a complex isotropic skin around a wellbore on the convergence factor has been examined and compared with previous results. The conventional model of a skin (finite radius and constant permeability change) may be a correct approximation in the case of a positive skin (permeability decrease near the well). But for negative skin very high convergence factors (up to or even over 10) can be obtained if the complex developed skin region varies continuously in permeability. This does not occur in the case of a conventional skin, for which the upper limit is 4.

The impact of a conventional and a complex skin on a single-well capture zone has been investigated. In both cases, the effect of the skin is generally not significant enough to invalidate the classical result. However, if the well is located in a natural zone of dimension 100–1000 m that is more permeable than the rest of the aquifer, the capture zone may be much smaller than that predicted by assuming a homogeneous aquifer.

The more important application is probably in the analysis of piezometric data and tracer transport data around large-diameter wells or underground drifts. In these cases, the flow around the well or drift may be significantly distorted by the combination of radial and regional flow, as well as by the possible permeability change due to the stress redistribution around the hole. Many plots given in this paper are examples of what may be observed in the field, and they will be helpful in the analysis of such field data. In a real field study, the problem would be to fit some parameters (radial and regional flow, hydromechanical and dispersive properties of the medium around the hole) to the flow model provided in the present paper in order to match the field data as closely as possible. That inverse problem would not be straightforward or unique, and has to be done numerically by trial and error.

The semi-analytic results provided in this paper will provide an appropriate background for field data analysis, and also provide useful guidelines for detailed numerical modeling.

NOTATION

$a(r)$, $b(r)$ auxiliary functions defined in (10)
e aquifer thickness
h depth of a drift under water table
i_w apparent hydraulic gradient at a cemented drift
i_∞ hydraulic gradient for the unperturbed regional flow

l	length of the convective path from a point to the drift
m	mass of injected tracer
p_0	overburden stress
q	dimensionless pumping rate
r	radial coordinate (from well or drift axis)
r_s	radius at which the stagnation point is located
r_{s_0}	value of r_s for a homogeneous aquifer
s	skin factor
t_c	convective travel time to the drift
u	complex skin parameter (see (2))
C	tracer concentration
D	longitudinal dispersion
$K(r)$	hydraulic conductivity (isotropic skin)
K_0	hydraulic conductivity at no stress
K_∞	hydraulic conductivity of the unperturbed aquifer
K_d	hydraulic conductivity of a conventional skin
K_l	limit value of K at high stress
$K_r(r)$	radial hydraulic conductivity (anisotropic skin)
$K_\theta(r)$	tangential hydraulic conductivity (anisotropic skin)
$\hat{K}(r)$	$= \sqrt{K_\theta(r) K_r(r)}$
$\overline{\overline{K}}$	hydraulic conductivity (tensor)
Q	pumping rate
Q_c	critical value of pumping rate (defined by (21))
R_d	outer radius of a conventional skin
R_p	penetration radius of a complex skin
R_w	radius of the well or drift
$V(r,\theta)$	local Darcy velocity (absolute value)
V_p	local pore velocity
$<V_p>$	mean pore velocity along a path
$V_r(r,\theta)$	radial component of Darcy velocity
$V_\theta(r,\theta)$	tangential component of Darcy velocity
V_w	apparent Darcy velocity at the well (drift)
V_∞	Darcy velocity of the unperturbed regional flow
$\alpha(r)$	$= \sqrt{K_\theta(r)/K_r(r)}$
α_L	longitudinal dispersivity
γ	complex skin parameter (see (2))
θ	azimuthal coordinate
$\phi(r,\theta)$	hydraulic potential
$\psi(r,\theta)$	stream function
σ, τ	stress components
ω	kinematic porosity

Acknowledgments. The review and comments from J. Noorishad and R. W. Zimmerman of Lawrence Berkeley Laboratory were highly appreciated. This work is jointly supported by Office of Drinking Water, U. S. Environmental Protection Agency (Interagency Agreement DW89931336-01-6), and Office of Energy Research, Office of Basic Energy Sciences, Engineering and Geosciences Division of the U. S. Department of Energy under contract number DE-AC03-76SF00098.

REFERENCES

Aubertin, G., Benderitter, Y., Cordier, E., Doillon, F., Fabris, H., Gable, R., Gaillard, B., Ledoux, E., and De Marsily, G. (1987). Experimental measurement of the natural flow velocity of the Dogger geothermal aquifer in the Paris basin. *Bull. Soc. Géol. France*, vol. 8, t. III, no. 5, p. 991-1000.

Bidaux, P., and Tsang, C. F. (1989). An analytic solution relating wellbore and formation velocities with application to tracer dilution problem. Proc., Conference "New Field Techniques," Dallas, Texas, March 20-23, 1989, p. 585-604. National Water Well Association.

Cacas, M. C., Ledoux, E., and De Marsily, G. (1987a). Etude de l'effet d'échelle en milieu fissuré - Phase 2A: Etude des écoulements sur le site de Fanay-Augères - Rapport final - 2è partie - Interprétation et modélisation. Ecole Nationale Supérieure des Mines de Paris, Fontainebleau, ref. LHL/RD/87/5, March 1987 (C. E. A., report to the Commission of the European Communities).

Cacas, M. C., Ledoux, E., and De Marsily, G. (1987b). Etude de l'effet d'échelle en milieu fissuré - Phase 2B: Etude des écoulements sur le site de Fanay-Augères - Rapport final - 2è partie - Modélisation des essais de traçage. Ecole Nationale Supérieure des Mines de Paris, Fontainebleau, ref. LHL/RD/87/74, March 1987 (C. E. A., report to the Commission of the European Communities).

Carslaw, H. S., and Jaeger, J. C. (1959). Conduction of Heat in Solids. Oxford University Press, New York, 1959, 510 p.

Drost, W., Klotz, D., Koch, A., Moser, H., Neumaier, F., and Rauert, W. (1968). Point dilution methods of investigating groundwater flow by means of radioisotopes. *Water Resour. Res.*, vol. 4, no. 1, p. 125-146.

Gangi, A. F. (1978). Variation of whole and fractured porous rock permeability with confining pressure. *Int. J. Rock Mech. Min. Sci.*, vol. 15, p. 249-257.

Holt, R. M. (1989). Permeability reduction induced by a non-hydrostatic stress field. Paper SPE 19595, 64th Annual Technical Conference and Exhibition of the Society of Petroleum Engineers, San Antonio, Texas, October 8-11, 1989.

Hubbert, M. K. (1940). Theory of groundwater motion. *J. Geology*, XLVIII, 8, p. 785-944.

Jaeger, J. C., and Cook, N. G. W. (1969). Fundamentals of Rock Mechanics. Methuen & Co. Ltd., London, 1969, 514 p.

Javandel, I., and Tsang, C. F. (1986). Capture-zone type curves: A tool for aquifer cleanup. *Groundwater*, vol. 24, no. 5, p. 616-625.

McLinn, E. L., and Palmer, C. D. (1989). Laboratory testing and comparison of specific-conductance and electrical-resistivity borehole-dilution devices. Proc., Conference "New Field Techniques," Dallas, Texas, March 20-23, 1989, p. 465-485. National Water Well Association.

Neretnieks, I. (1987). Channeling effects in flow and transport in fractures rocks - some recent observations and models. GEOVAL-87, International Symposium, Stockolm, Sweden, April 7-9, 1987.

Tsang, Y. W., and Witherspoon, P. A. (1981). Hydromechanical behavior of a deformable rock fracture subject to normal stress. *J. Geophys. Res.*, vol. 86, no. B10, p. 9287-9298.

Wilson, C. R., Long, J. C. S., Galbraith, R. M., Karasaki, K., Endo, H. K., Dubois, A. O., McPherson, M. J., and Ramqvist, J. (1981). Geohydrological data from the macropermeability experiment at stripa, Sweden. Lawrence Berkeley Laboratory, Report LBL-12520, SAC-37.

TABLE 1A

plot label	u	γ	skin factor s	convergence factor Ξ
a	–4.15	1.	–2.	5.44
b	2.10	1.	4.	0.87
c	2.96	2.	4.	0.68
d	5.07	10.	4.	0.47

Value of parameters and calculated skin and convergence factors for complex isotropic wellbore skins described by equation (2).

TABLE 1B

stress	non-elastic deformation	skin factor s	convergence factor Ξ
no	no	0	2
yes	no	1.68	0.31
no	yes	–0.66	2.13
yes	yes	1.37	0.41

Value of skin and convergence factors around an underground drift, with K_r and K_θ given by (4.3) and (4.4). Stress-induced skin parameters are $K_0 = 10K_\infty = 100K_l$. Parameters induced by inelastic deformation are $u = -2$ and $\gamma = 20$.

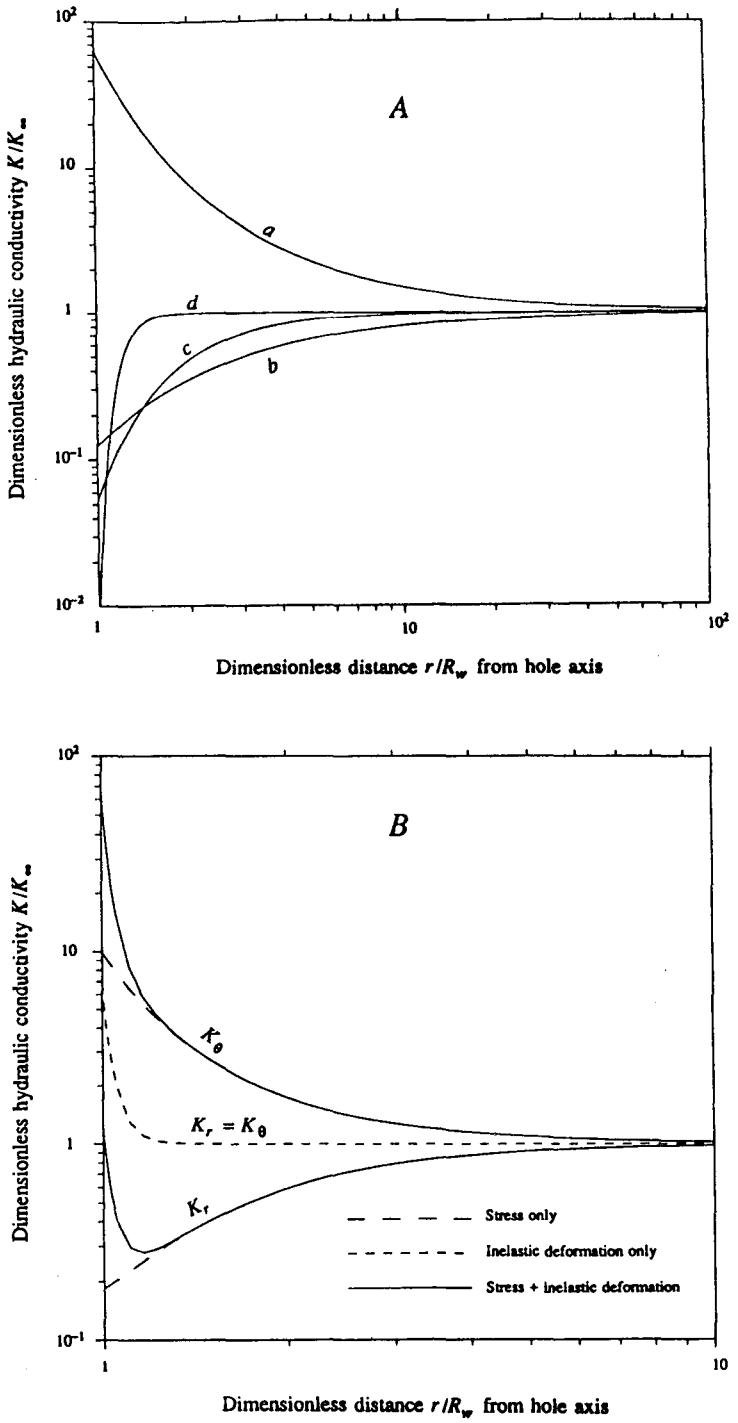

Fig. 1. (*A*) Examples of radial variation of hydraulic conductivity in a complex isotropic skin around a wellbore, using equation (2). Parameters corresponding to curves *a*, *b*, *c*, and *d* are given in Table 1*A*. (*B*) Schematic radial variations of the principal values K_r and K_θ of hydraulic conductivity in the complex radially anisotropic region around an underground drift, showing result from stress redistribution only, permanent inelastic deformation caused by excavation, and both stress redistribution effect and non-elastic deformation.

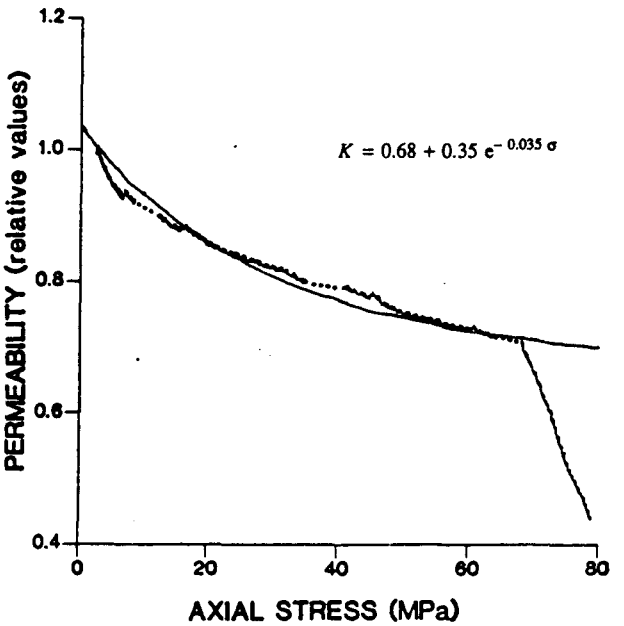

Fig. 2. Exponential fitting to the experimental variations of rock hydraulic conductivity K as a function of stress σ for Wildmoor sandstone (data from Holt, 1989).

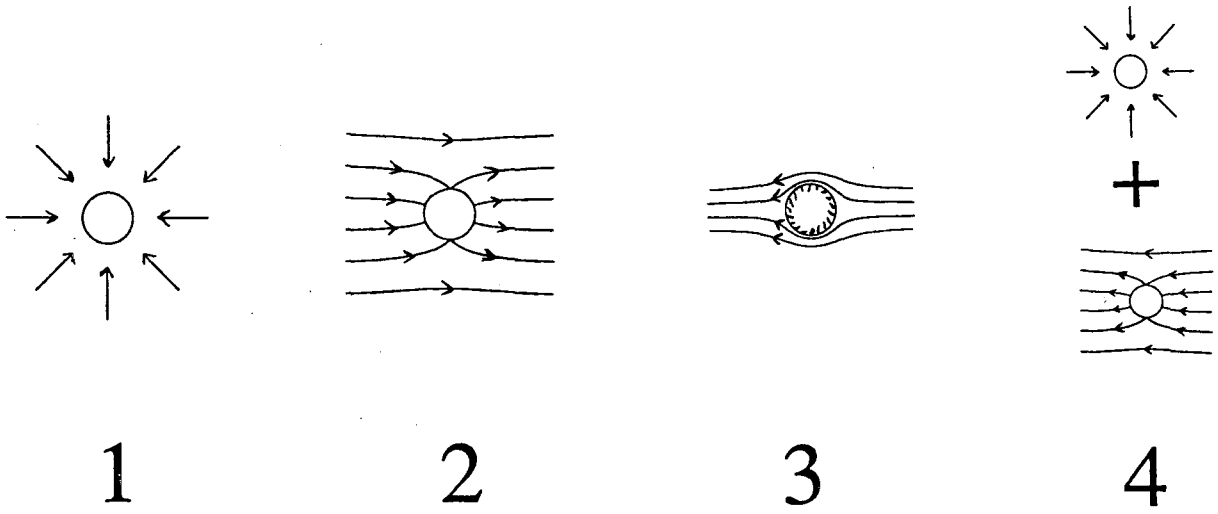

Fig. 3. The flow patterns studied.

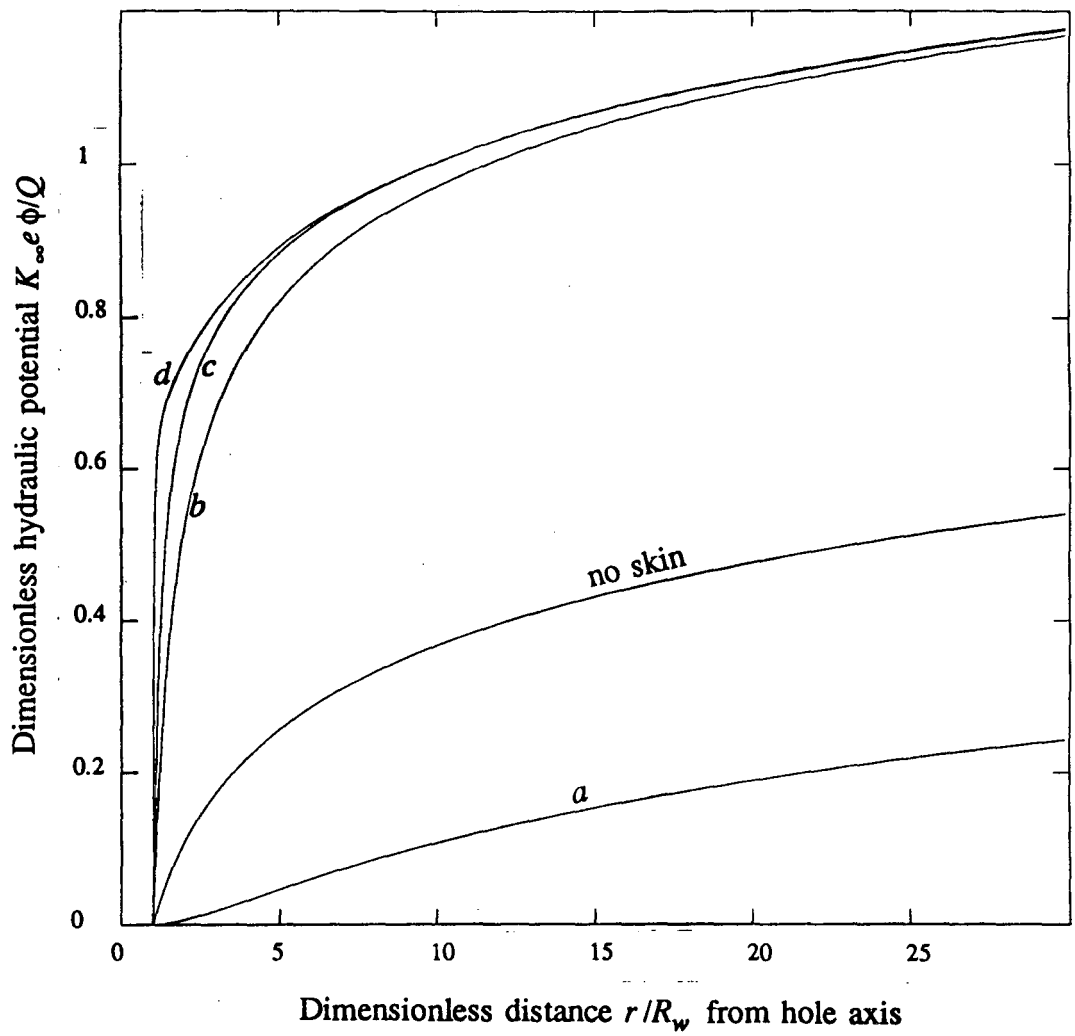

Fig. 4. Radial variations of the hydraulic potential for a purely convergent flow to a well with a complex skin. Plots *a* to *d* refer to the configurations so labeled in Figure 1*A*. Note that the configurations *b* to *d*, corresponding to the same skin factor s=4, behave differently close to the well but give the same potential values at distances more than about 20 times its radius.

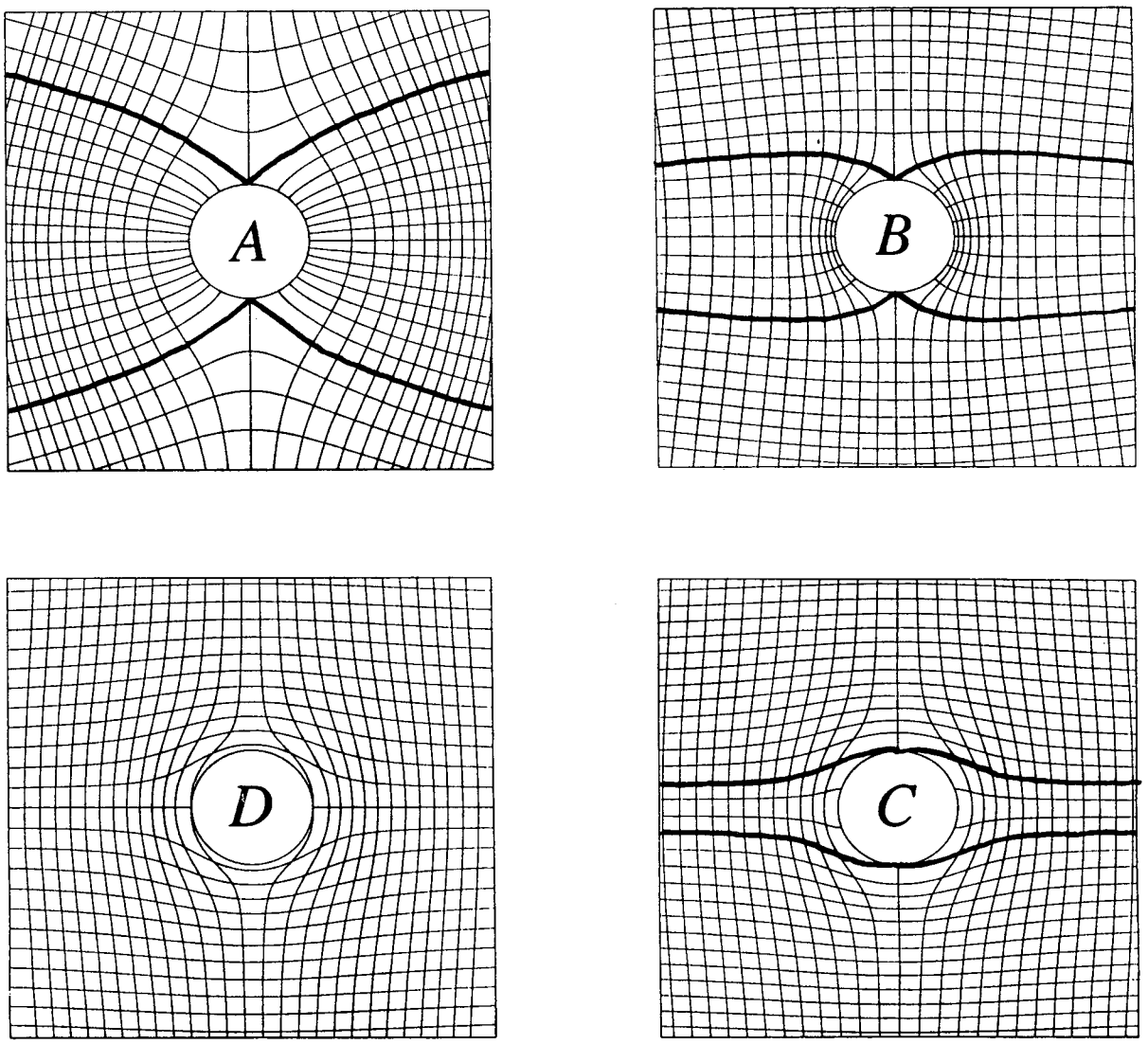

Fig. 5. Equipotentials and streamlines for regional flow without pumping around a hole with a complex skin. (*A*) developed wellbore (case *a* of Figure 1*A*). (*B*) Damaged wellbore (case *b* of Figure 1*A*). (*C*) Open drift. (*D*) Cemented drift with stress and inelastic deformation effects (solid lines in Figure 1*B*).

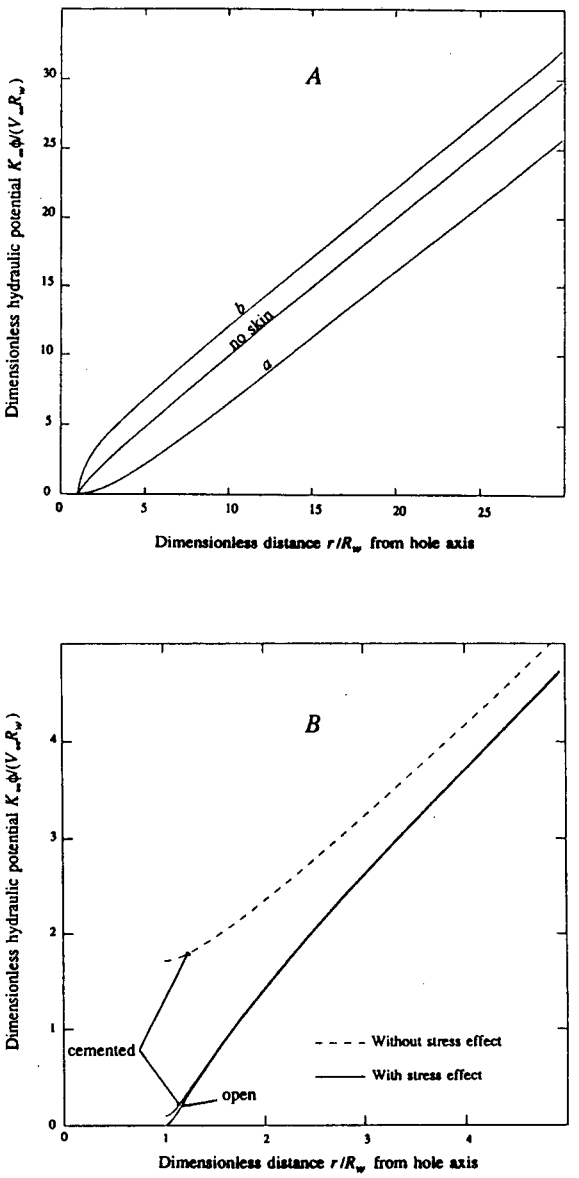

Fig. 6. Radial variation of the hydraulic potential in the direction θ=0 (upstream, parallel to the flow) for regional flow without pumping/injecting. (*A*) Wellbore with a complex isotropic skin (*a*–*b* refer to the configurations labeled *a*–*b* in Figure 1*A*). (*B*) Open or cemented drift with or without stress effect (configurations of Figure 1*B*, flow types 2 and 3).

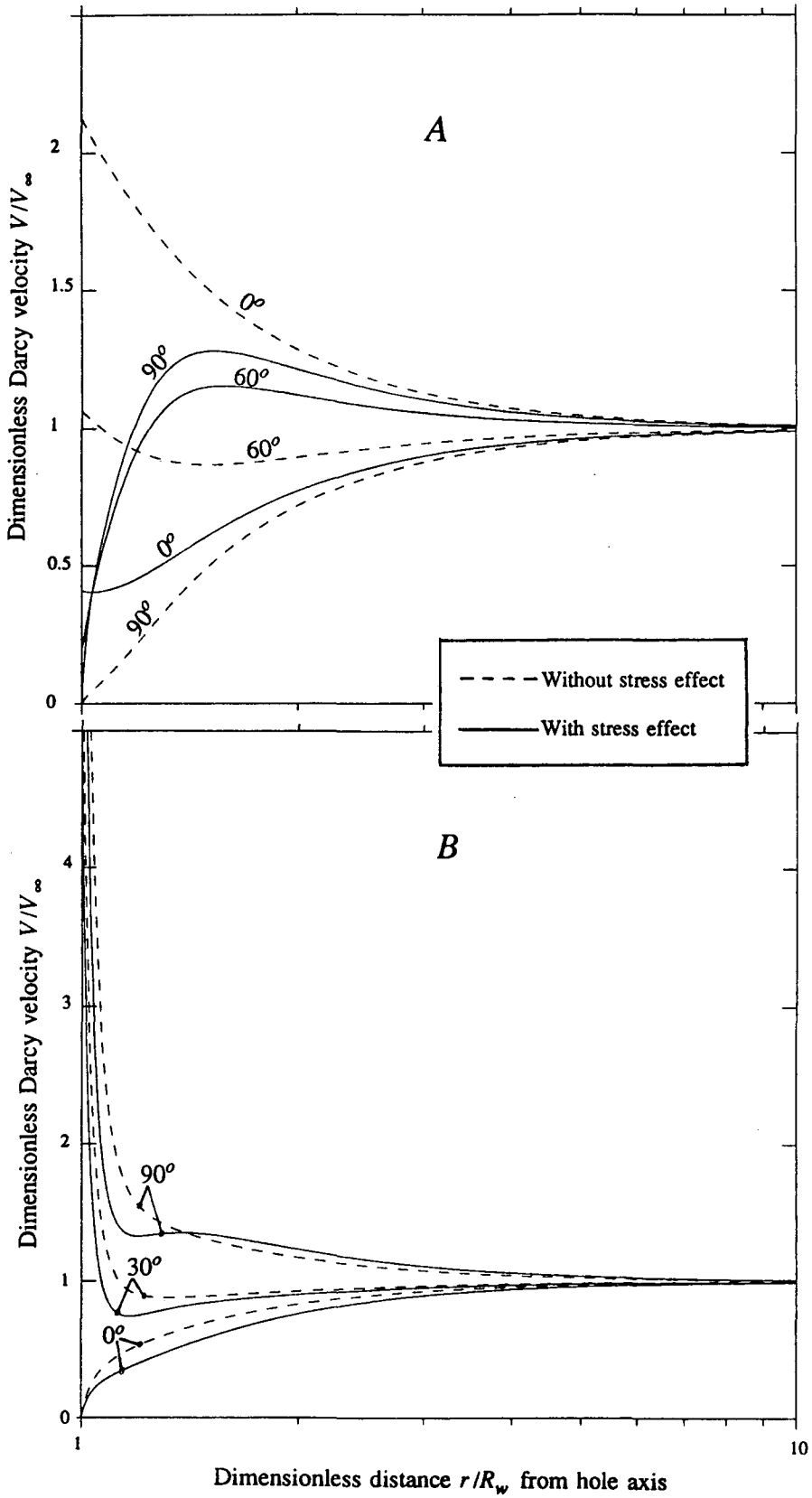

Fig. 7. Radial variation of local Darcy velocity, in three azimutal directions, for regional flow without source term around a drift with or without stress effect: (*A*) open drift, (*B*) cemented drift.

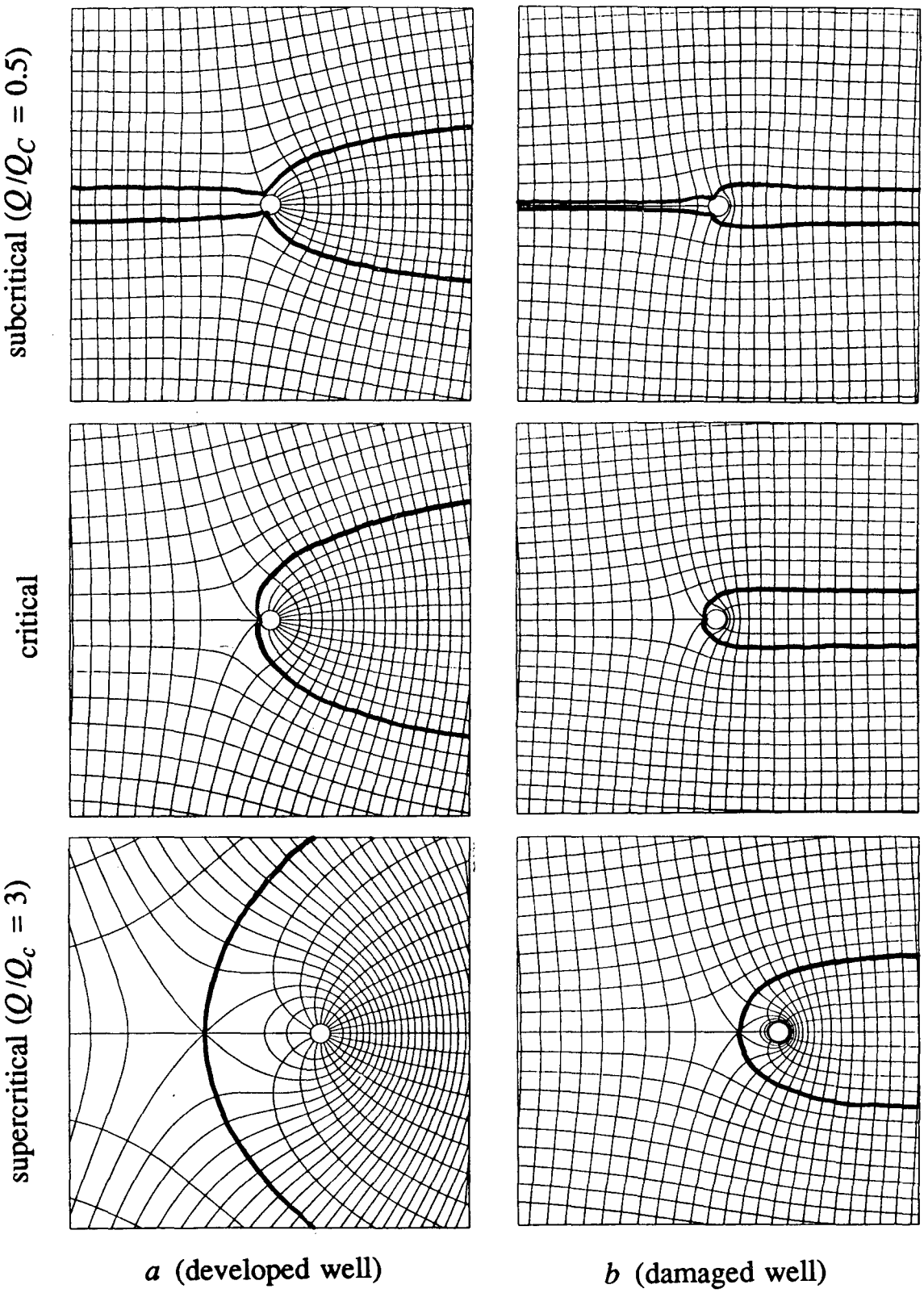

Fig. 8. Equipotentials and streamlines for regional flow around a producing well with a complex isotropic skin, showing the cases of subcritical, critical, and supercritical pumping rates for configurations *a* and *b* of Figure 1*A*. Note that for a given value of pumping rate, the flow may be either sub- or supercritical, according to the skin: the pumping rates for subcritical flow in the developed well (top, left) and for supercritical flow in the damaged well (bottom, right) are about the same.

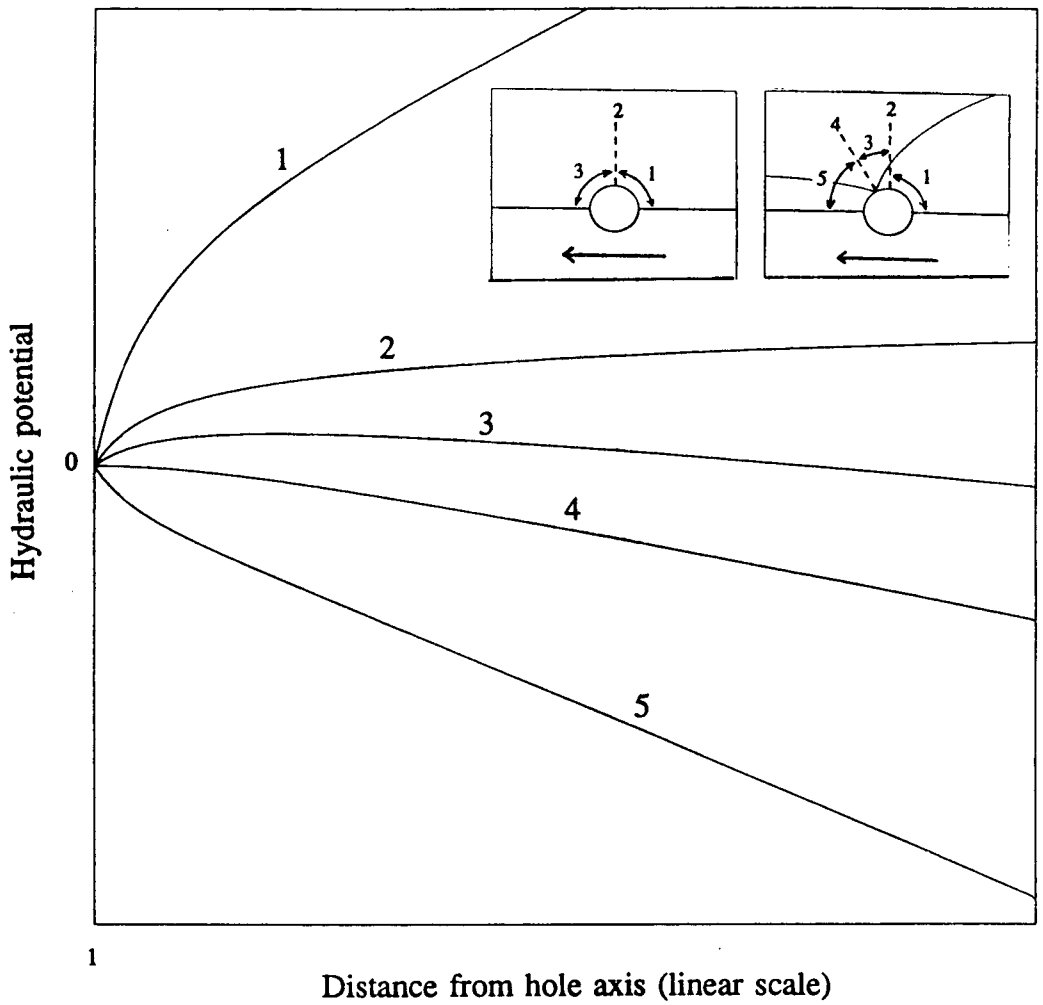

Fig. 9. Type curves of hydraulic potential profile for regional flow around a producing well with a complex skin. The labels refer to the direction in which the corresponding curve is observed. Curves 4 and 5 can exist only if the pumping rate is subcritical.

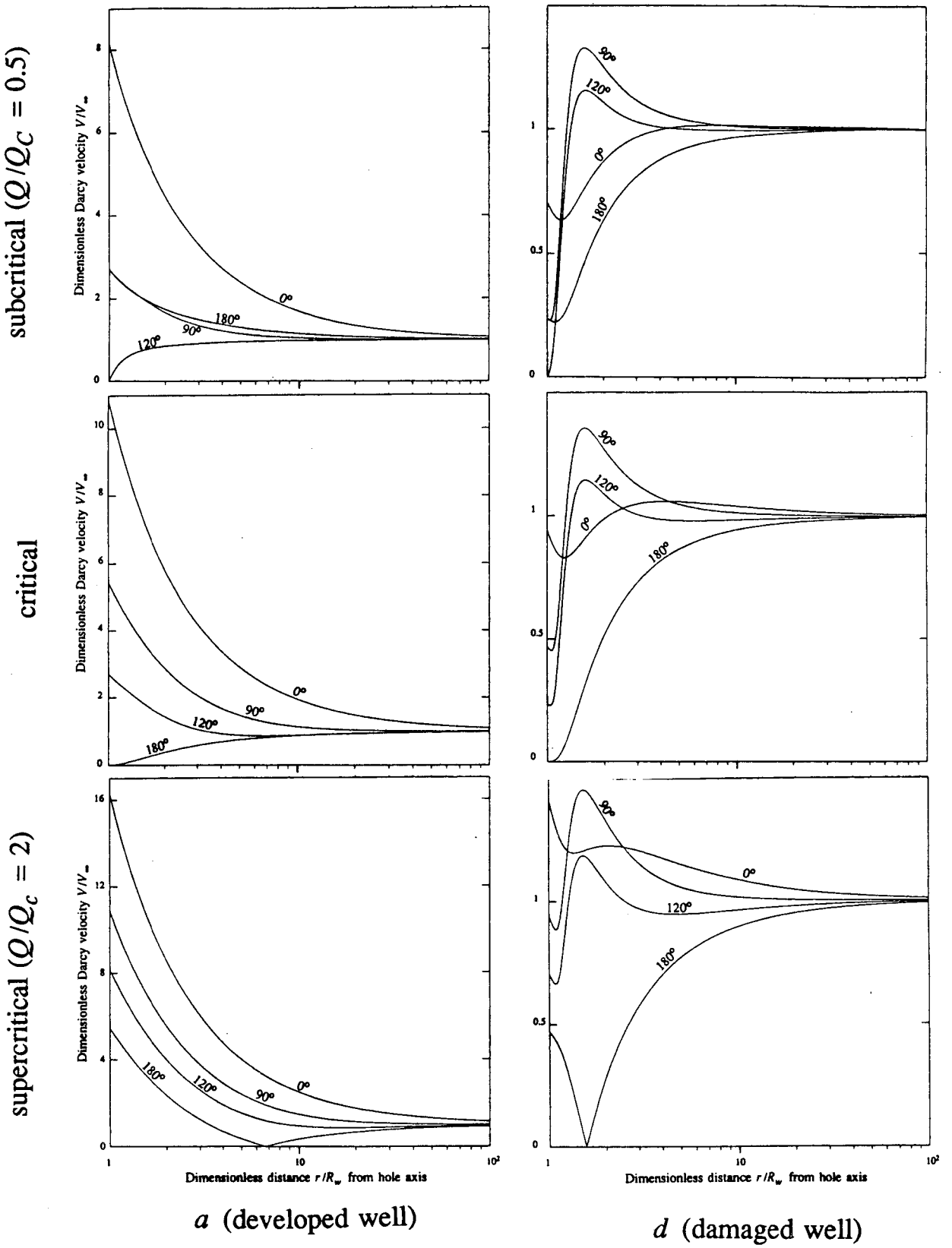

Fig. 10. Darcy velocity profiles in various azimuthal directions for regional flow around a producing well with a complex skin, showing the cases of subcritical, critical, and supercritical pumping rates for configurations *a* (developed well), and *d* (damaged well). The figures labeling the plots indicate the angular orientation θ of the corresponding profile in degrees (θ=0 is parallel to the regional flow, upstream).

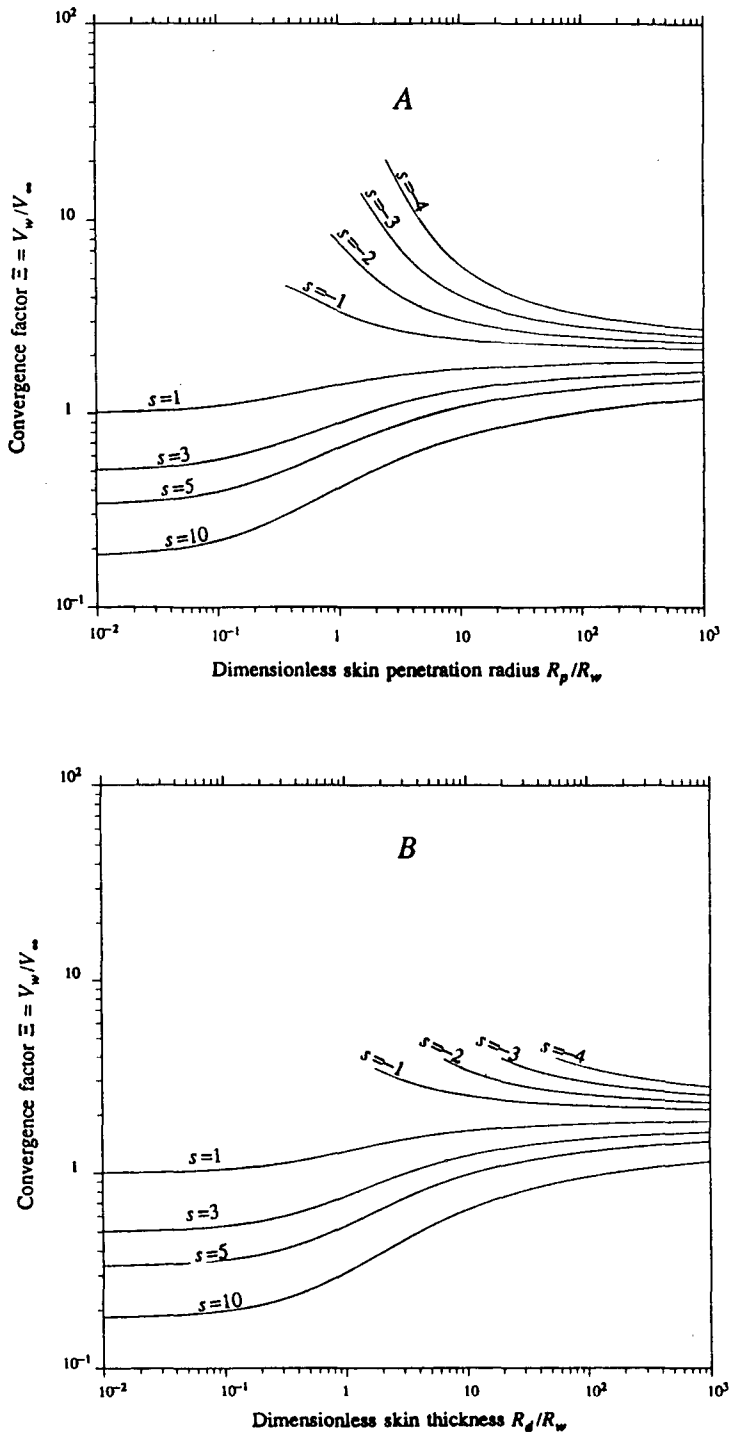

Fig. 11. (*A*) Convergence factor as a function of the penetration radius R_p for various skin factors in the case of a complex skin described by expression (2). (*B*) Convergence factor as a function of the skin thickness for various skin factors in the case of a conventional skin (outer radius R_d, constant hydraulic conductivity K_d).

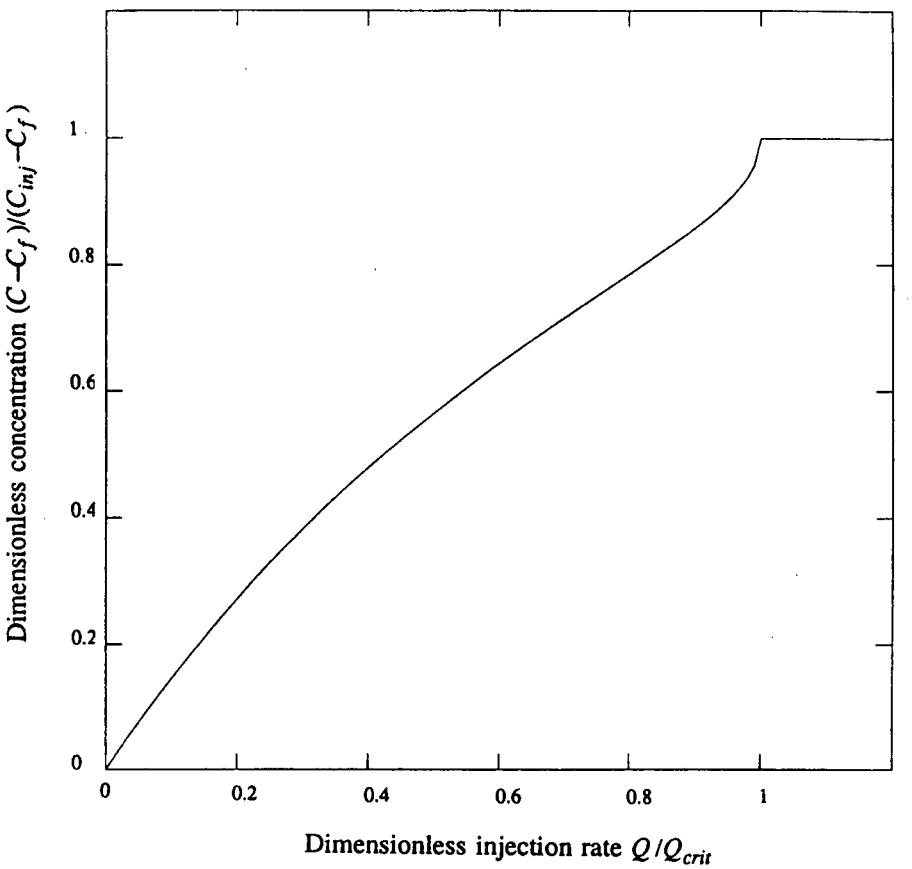

Fig. 12. Effective concentration entering the formation as a function of the injection flow rate for a tracer injected in a borehole with regional flow.

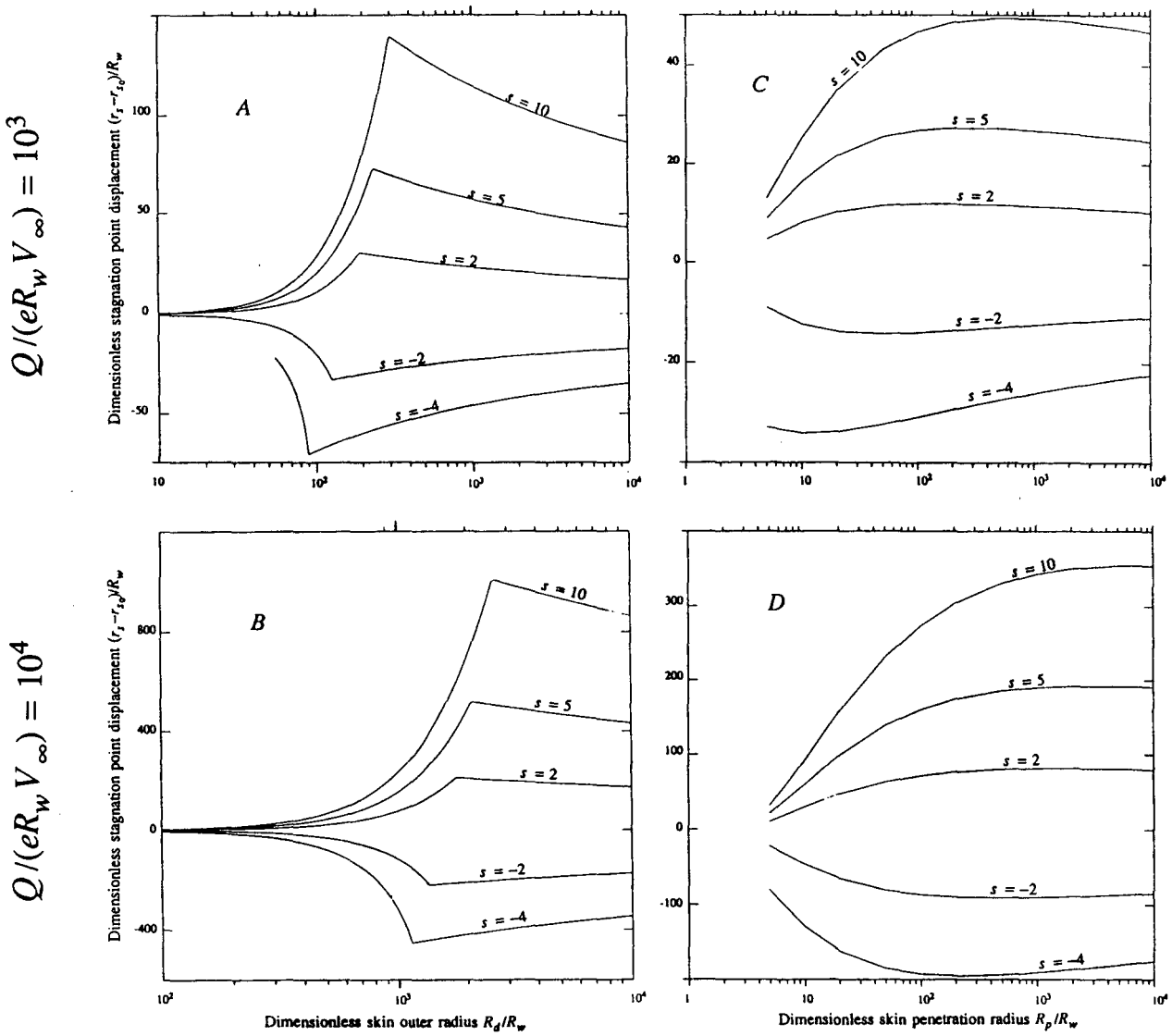

Fig. 13. Stagnation point displacement $r_s - r_{s_0}$ caused by the presence of a skin in the case of pumping in an aquifer with regional flow: influence of the size of the skin at various skin factors.

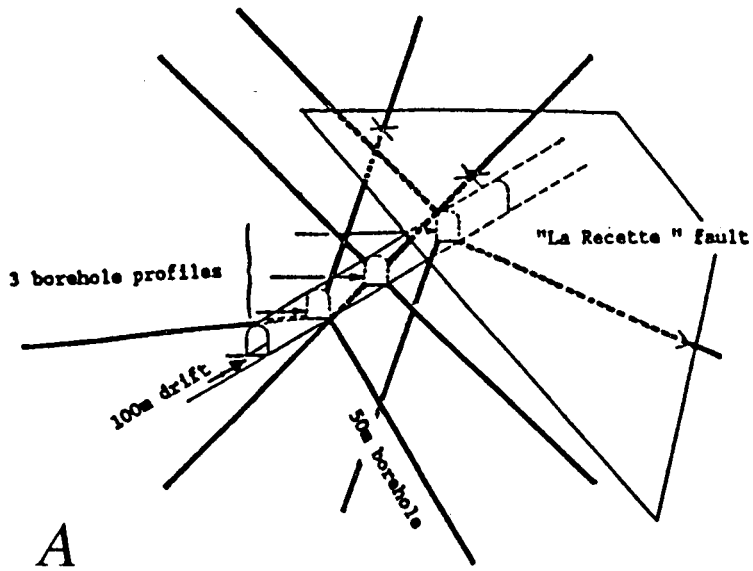

Figure from the BRGM Report 87 SGN 502 STO (1987)

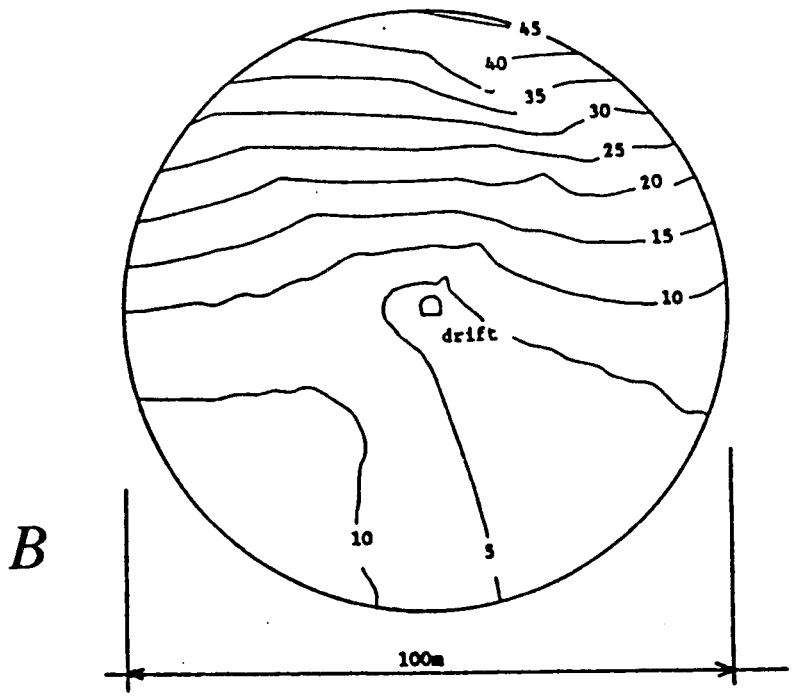

Fig. 14. Acquisition of hydraulic potential data in observation wells to study the flow around an underground drift: Fanay-Augères, France (from Cacas et al., 1987): (*A*) position of drift and boreholes, (*B*): observed piezometric heads (in m).

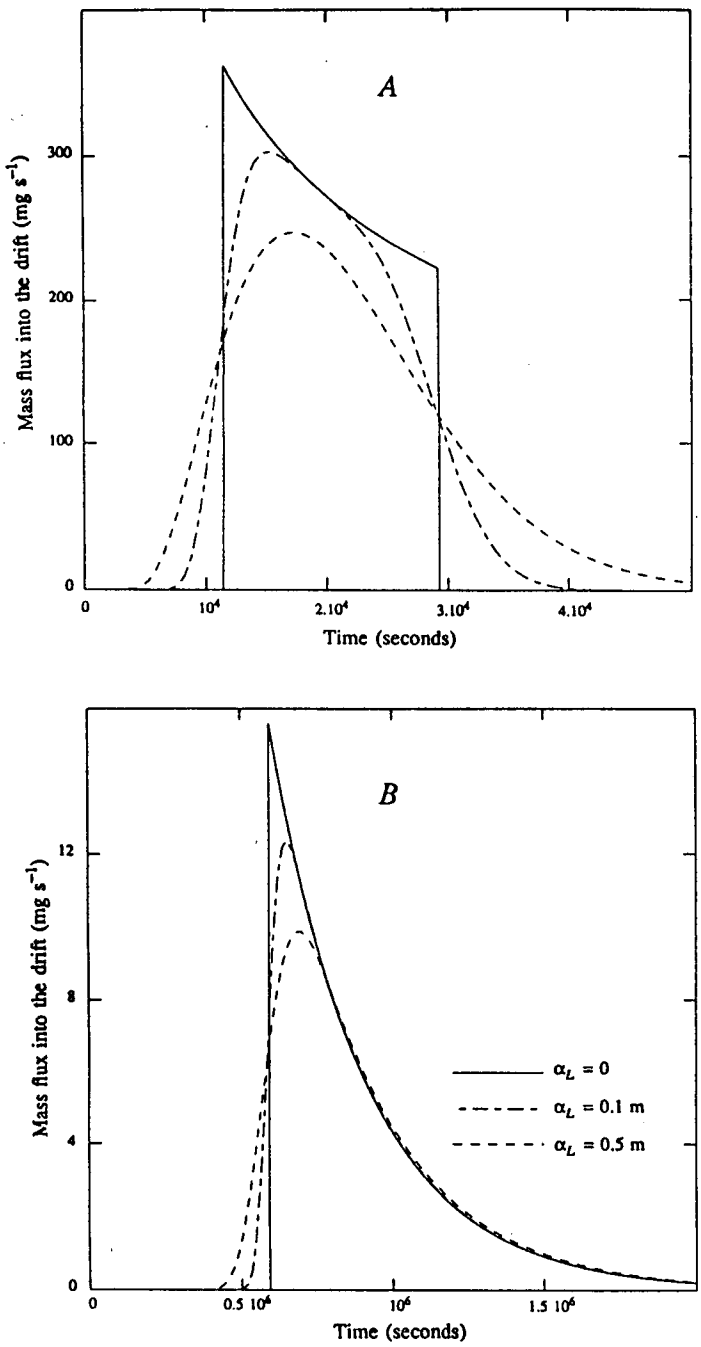

Fig. 15. Simulated tracer breakthrough curves for the injection of a tracer in a borehole between two packers located at distances r_1 and r_2 from the drift wall. The borehole makes an angle $\theta = 90°$ with the direction of the regional flow, and the configuration parameters are: drift radius $R_w = 1$ m, no skin, kinematic porosity $\omega = 10^{-2}$, Darcy velocity of regional flow $V_\infty = 10^{-6}$ m s^{-1}, flow rate to the drift $Q = 2\text{x}10^{-4}$ m^3 s^{-1} for 1 m length, injected mass of tracer $m_0 = 5$ kg. The stagnation point is located at a distance $r_s = 31.8$ m from the drift axis. (*A*) Total recovery (injection interval between 10 and 15 m, entirely inside the capture zone). (*B*) Partial recovery (injection interval between 44 and 49 m, extending beyond the capture zone).

LAWRENCE BERKELEY LABORATORY
TECHNICAL INFORMATION DEPARTMENT
1 CYCLOTRON ROAD
BERKELEY, CALIFORNIA 94720